

CERN-EP-2024-213
08 August 2024

Measurement of exclusive J/ψ and $\psi(2S)$ production at $\sqrt{s} = 13$ TeV

LHCb collaboration[†]

Abstract

Measurements are presented of the cross-section for the central exclusive production of $J/\psi \rightarrow \mu^+\mu^-$ and $\psi(2S) \rightarrow \mu^+\mu^-$ processes in proton-proton collisions at $\sqrt{s} = 13$ TeV with 2016–2018 data. They are performed by requiring both muons to be in the LHCb acceptance (with pseudorapidity $2 < \eta_{\mu^\pm} < 4.5$) and mesons in the rapidity range $2.0 < y < 4.5$. The integrated cross-section results are

$$\sigma_{J/\psi \rightarrow \mu^+\mu^-}(2.0 < y_{J/\psi} < 4.5, 2.0 < \eta_{\mu^\pm} < 4.5) = 400 \pm 2 \pm 5 \pm 12 \text{ pb},$$

$$\sigma_{\psi(2S) \rightarrow \mu^+\mu^-}(2.0 < y_{\psi(2S)} < 4.5, 2.0 < \eta_{\mu^\pm} < 4.5) = 9.40 \pm 0.15 \pm 0.13 \pm 0.27 \text{ pb},$$

where the uncertainties are statistical, systematic and due to the luminosity determination. In addition, a measurement of the ratio of $\psi(2S)$ and J/ψ cross-sections, at an average photon-proton centre-of-mass energy of 1 TeV, is performed, giving

$$\frac{\sigma_{\psi(2S)}}{\sigma_{J/\psi}} = 0.1763 \pm 0.0029 \pm 0.0008 \pm 0.0039,$$

where the first uncertainty is statistical, the second systematic and the third due to the knowledge of the involved branching fractions.

For the first time, the dependence of the J/ψ and $\psi(2S)$ cross-sections on the total transverse momentum transfer is determined in pp collisions and is found consistent with the behaviour observed in electron-proton collisions.

Submitted to sciPost Physics

© 2024 CERN for the benefit of the LHCb collaboration. [CC BY 4.0 licence](https://creativecommons.org/licenses/by/4.0/).

[†]Authors are listed at the end of this paper.

1 Introduction

Deep inelastic scattering of leptons off protons provided the first proof that hadrons are not elementary but rather composed of quarks [1,2]. It is an essential tool to determine parton distribution functions (PDFs) inside protons, which are required to make cross-section predictions at hadron colliders. However, charged leptons interact electromagnetically and only probe the density of the quarks, which are charged. The densities of the neutral gluons must be inferred, which can be done by studying how the quark PDFs evolve with the scale set by the mass of the exchanged virtual photon. These PDFs are determined in fits [3–5] to multiple measurements, including notably $e^\pm p$ scattering at HERA [6,7], and LHCb measurements of vector boson [8–11] and heavy-quark [12–15] production. Due to a lack of data at low x , the fraction of hadron momentum carried by the parton, the uncertainties attributed to the gluon PDFs are large at low x and are even compatible with an unphysical decrease of the gluon density with x [16]. Other methods are thus required to access the gluonic PDF.

Central exclusive vector-meson production (CEP) in pp collisions is the quasi-elastic production of a single meson, leaving the protons intact. Exclusive charmonium production results from the conversion of a virtual photon close to its mass shell into a $c\bar{c}$ pair, which hadronises into a J/ψ or $\psi(2S)$ meson. These processes probe the gluonic PDF at the scale of the charm quark mass. The exclusivity of the process requires that, at leading order, two gluons are exchanged with the target hadron. Thus the cross-section approximately scales as gluon density squared [17–20]. The process and the main backgrounds are depicted in Fig. 1.

Exclusive scattering processes also give access to the total transverse momentum transfer Δt , the square of the difference between the momenta of the incoming and outgoing proton, which is a Fourier conjugate to the impact parameter between two colliding hadrons. As such, the Δt spectra are sensitive to the spatial distribution of colour charge [21]. Several predictions (see *e.g.* Ref. [18]) calculate the exclusive production cross-section at $\Delta t \sim 0$. The cross-section falls exponentially versus Δt with a slope determined experimentally, which can be used to infer the total exclusive cross-section. In the present paper, this slope is determined in ten intervals of rapidity for the J/ψ and $\psi(2S)$ mesons. As the outgoing protons are not detected at LHCb, Δt is not directly accessible and the transverse momentum squared, p_T^2 , of the charmonium state is used as a proxy.

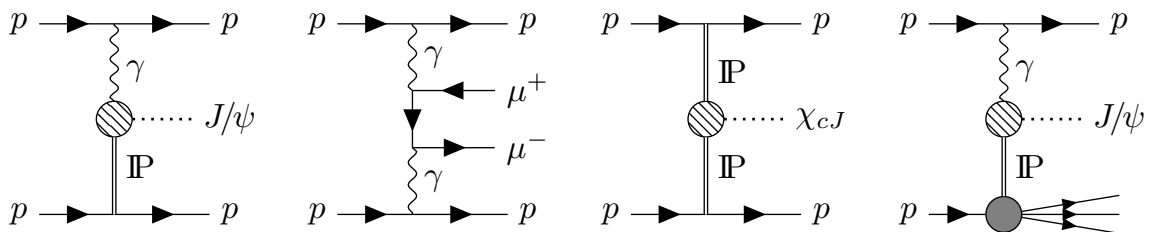


Figure 1: Feynman diagrams for signal and background processes. From left to right: signal CEP J/ψ photoproduction, where IP stands for a colourless superposition of gluons, sometimes referred to as a pomeron; continuum dimuon production; exclusive χ_c ($J = 0, 1, 2$) production via double pomeron exchange; inelastic pp collision where a proton dissociates.

The photoproduction cross-section of a charmonium state is sensitive to the radial wave function of the charmonium state in a region where the $\psi(2S)$ wave function has a radial node but the J/ψ wave function does not. As a result, the $\psi(2S)$ photoproduction cross-section is expected to be suppressed with respect to that of J/ψ mesons [22–31]. With many theoretical uncertainties cancelling, predictions for the ratio of $\psi(2S)$ and J/ψ cross-sections can be determined more precisely than the individual cross-sections.

Exclusive J/ψ and $\psi(2S)$ production in pp collisions at the LHC have previously been measured at centre-of-mass energies of $\sqrt{s} = 7$ TeV [32–34] and 13 TeV [35]. Exclusive double-charmonium [36] and Υ [37] production have been measured at 7 and 8 TeV, and that of $J/\psi\phi$ at 13 TeV [38]. Charmonia production has also been studied in ultra-peripheral $p\text{Pb}$ [39] and PbPb [40–42] collisions.

The previous LHCb measurements have been used to update PDF fits [19, 43], and thus improve predictions of J/ψ and Υ CEP cross-sections [18, 44, 45]; make predictions [46–52] for ultra-peripheral photoproduction processes at RHIC [53, 54] and the LHC [34, 42, 55, 56]; determine the meson-proton scattering length [57] and extract the proton mass radius from the J/ψ and $\psi(2S)$ cross-sections [58]. Based on these cross-sections, Ref. [59] claims that LHCb data show evidence of gluon saturation, *i.e.* the slowing down of the growth of gluon densities as x decreases due to gluon emission and recombination balancing each other, while the authors of Ref. [45] disagree. Such effects would usually be expected in heavy-ion collisions.

This paper presents a measurement of exclusive J/ψ and $\psi(2S)$ production in proton-proton collisions at $\sqrt{s} = 13$ TeV in the forward direction, in ten intervals of rapidity between 2.0 and 4.5. The data used were collected with the LHCb detector at the LHC between 2016 and 2018, corresponding to an integrated luminosity of 4.4 fb^{-1} , which is twenty times larger than that used in Ref. [35]. This larger sample permits a first measurement of the $\psi(2S)$ cross-section in the same rapidity intervals as for the J/ψ cross-section, and thus the determination of their ratio as a function of rapidity.

2 Detector, simulation and data sample

The LHCb detector [60, 61] is a single-arm forward spectrometer covering the pseudorapidity range $2 < \eta < 5$, designed for the study of particles containing b or c quarks. The detector includes a high-precision tracking system consisting of a silicon-strip vertex detector (VELO) surrounding the pp interaction region [62], a large-area silicon-strip detector located upstream of a dipole magnet with a bending power of about 4 T m, and three stations of silicon-strip detectors and straw drift tubes [63] placed downstream of the magnet. The tracking system provides a measurement of the momentum, p , of charged particles with a relative uncertainty that varies from 0.5% at low momentum to 1.0% at 200 GeV/ c . Photons are identified by a calorimeter system consisting of scintillating-pad and preshower detectors (SPD), and electromagnetic and hadronic calorimeters. Muons are identified by a system composed of alternating layers of iron and multiwire proportional chambers [64].

The pseudorapidity coverage of the LHCb detector is extended by the HERSCHEL system, composed of forward shower counters consisting of five planes of scintillators with three planes at 114, 19.7 and 7.5 m upstream of the interaction point, and two downstream at 20 and 114 m. At each location, there are four quadrants of scintillators,

whose information is recorded in every beam crossing by photomultiplier tubes, giving a total of 20 channels in HERSCHEL [65]. These are calibrated using data taken without beams circulating at the end of each LHC fill [66]. The pseudorapidity ranges covered by the VELO and HERSCHEL are different. For the VELO the region is $-3.5 < \eta < -1.5$ and $2 < \eta < 5$, and for HERSCHEL the region is $-10 < \eta < -5$ and $5 < \eta < 10$.

The online event selection is performed by a trigger [67] that consists of a hardware stage, based on information from the calorimeter and muon systems, followed by a software stage, which applies a full event reconstruction. The distinct signature of CEP events is their low multiplicity. Consequently, at the hardware stage, the trigger selects events containing at least one muon with $p_T > 192 \text{ MeV}/c$ and fewer than 20 hits in the SPD detector. At the software stage events are selected if they contain two muons with $p_T > 400 \text{ MeV}/c$, fewer than 10 tracks in the VELO, of which at most four are reconstructed in the backward direction. A sample used for the determination of trigger, reconstruction and particle identification (PID) efficiencies is collected requiring a single muon with $p_T > 500 \text{ MeV}/c$ and the same multiplicity requirements as for the default selection.

The data used were collected between July 2016 and October 2018. The early 2016 data are not used as relevant trigger selections were not yet included. Data from the last month of data taking in 2018 is also discarded as it was affected by a noisy SPD readout board, which biases the number of SPD hits in low-multiplicity events.

Offline, events are required to contain only the two muon candidates, which should be of good quality, and identified as such, which implies that their momentum exceeds $3 \text{ GeV}/c$, the threshold to cross the calorimeter and reach the muon system. The event should contain no additional tracks in the VELO, and no photons other than those that are consistent with being radiated from the passage of muons through the detector material.

The muons from CEP signal J/ψ decays are well outside of the HERSCHEL acceptance; these counters are used to veto charged particles from the proton dissociating. The CEP cross-section measurements are performed with events that contain no such additional particles, *i.e.* HERSCHEL signals consistent with noise. The remaining events are retained for background studies. The HERSCHEL response is described using a discriminating χ^2 -like variable that quantifies the activity above noise taking into account correlations between the counters. The selection requirement is optimised using low-mass low- p_T^2 dimuon pairs, which are dominated by two-photon fusion.

Simulation is required to model the effects of the detector acceptance and the imposed selection requirements, and to study specific backgrounds. In the simulation, the charmonium candidate is generated and decayed using `SuperChic2` [68], with the exception of $\psi(2S) \rightarrow J/\psi X$ processes (where X is any combination of particles, mostly $\pi\pi$), for which the decay is handled by `EVTGEN` [69]. Final-state radiation is generated using `PHOTOS` [70]. The interaction of the generated particles with the detector, and its response, are implemented using the `GEANT4` toolkit [71] as described in Ref. [72]. The `ROOT` [73] and `LHCb` [74–76] software frameworks are used for the initial data preparation, while the analysis is written in the `PYTHON` language with standard scientific packages [77–82].

The total integrated luminosity of the used data sample is determined using empty-event counters calibrated by van der Meer scans and beam profile measurements [83] and is found to be $\mathcal{L}_{\text{int}} = 4.41 \pm 0.13 \text{ fb}^{-1}$. Due to the multiplicity requirements imposed in the trigger and the offline selection, only events with a single pp interaction are selected. The useful integrated luminosity is thus reduced by the fraction of events with a single

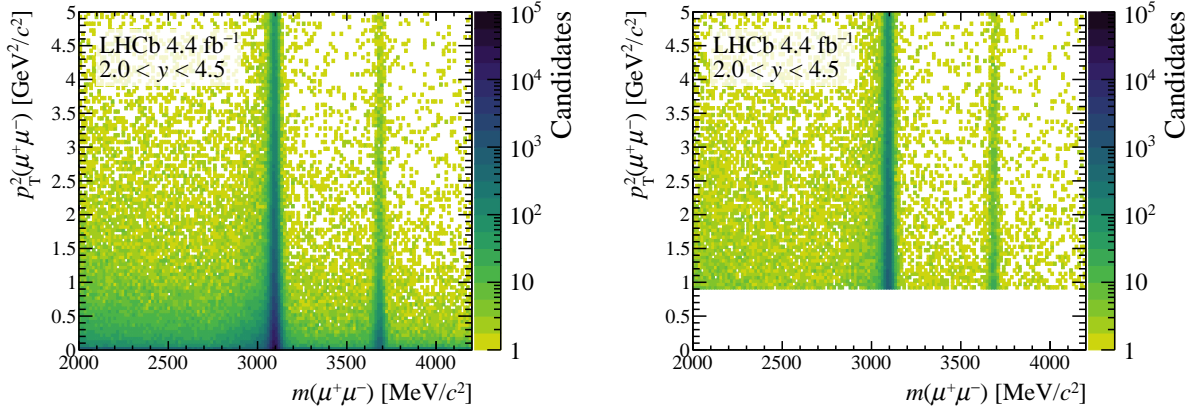


Figure 2: Two-dimensional mass- p_T^2 distributions for the (left) signal and (right) control samples.

interaction containing at least two VELO tracks. The number of such visible pp interactions per beam crossing, n , is assumed to follow a Poisson distribution, $P(n) = \mu^n e^{-\mu}/n!$, with mean μ . The fraction of useful integrated luminosity, $\mathcal{L}_{\text{int}}^{\text{eff}}$, corresponding to events with $n = 1$, is given by

$$f_{\mathcal{L}} = \frac{\mathcal{L}_{\text{int}}^{\text{eff}}}{\mathcal{L}_{\text{int}}} = \frac{P(n=1)}{\sum_{n=0}^{\infty} nP(n)} = \frac{\mu e^{-\mu}}{\sum_{n=0}^{\infty} n \frac{\mu^n e^{-\mu}}{n!}} = e^{-\mu}. \quad (1)$$

The value of μ depends on running conditions and it is determined in periods of up to one hour of stable running conditions [83]. In most running periods μ is close to 1.1, with variations of less than 10%, corresponding to an average $f_{\mathcal{L}} \simeq 0.33$. The corresponding useful integrated luminosity is $\mathcal{L}_{\text{int}}^{\text{eff}} = 1522 \pm 44 \text{ pb}^{-1}$, where the uncertainty is dominated by that on \mathcal{L}_{int} .

3 Two-dimensional signal fits

The primary challenge in this analysis is separation of the elastic CEP and inelastic proton-dissociation (PD) components, shown in Fig. 1. The latter consists of events where the proton dissociates, producing charged particles in the very forward acceptance. These are vetoed by the HERSCHEL requirement, which however is not perfect and thus leaves some PD backgrounds in the selected signal sample. The different p_T^2 distributions of PD and CEP charmonia are therefore also exploited. The properties of the PD component are determined from a control sample obtained by inverting the HERSCHEL veto, and requiring $0.9 < p_T^2 < 5.0 \text{ GeV}^2/c^2$, where the CEP contribution, which populates the low- p_T^2 region, is negligible.

Two other backgrounds are accounted for: QED continuum dimuon production and J/ψ feed-down from higher-mass charmonia, namely $\psi(2S)$, and $\chi_{cJ}(1P)$ ($J = 0, 1, 2$), referred to as χ_c below unless otherwise specified. Other feed-down contributions, such as those from Υ resonances or b hadrons, are negligible because of the VELO-tracks veto.

As there is a correlation between the dimuon mass and p_T^2 distributions for non-peaking backgrounds, a two-dimensional fit to the data in each of ten rapidity intervals is

performed. The considered regions are $2000 < m_{\mu^+\mu^-} < 4200 \text{ MeV}/c^2$ and $p_T^2 < 5 \text{ GeV}^2/c^2$. The relevant distributions are shown in Fig. 2. Overall, there are 566 095 events in the signal sample and 56 654 in the control sample.

The signal yields are determined in each rapidity interval by a two-dimensional unbinned extended maximum-likelihood fit [79, 80] in mass and p_T^2 . The fit model comprises the signal J/ψ and $\psi(2S)$ components; the continuum QED background; the $\psi(2S)$ and χ_c feed-downs; and the inelastic PD background. Prior to carrying out the fit in each rapidity interval, fits to the whole signal and control data samples (referred to as the full sample) are performed and their result are used to constrain nuisance parameters that cannot be determined accurately in low-yield rapidity regions, as described below.

The CEP and PD J/ψ and $\psi(2S)$ mass peaks are each modelled with a Gaussian function, modified to have power-law tails on both sides [84]. The difference in the means of the two Gaussian components is fixed according to the known mass difference of the two resonances [85]. Their widths are constrained to scale linearly with the energy release in the respective decays [86]. The tail parameters are shared between the two peaks and Gaussian-constrained to the values determined in the fits to the full sample.

The CEP p_T^2 shape is independent of the mass and is described by an exponential function, as expected by Regge theory [87] and measured in previous experiments, notably at HERA [88]. The slopes of the J/ψ and $\psi(2S)$ exponentials are left free to float in each rapidity interval.

The p_T^2 distribution of the PD J/ψ and $\psi(2S)$ mesons is modelled with a power-law function proportional to $(1 + (b_{\text{pd}}/n_{\text{pd}})p_T^2)^{-n_{\text{pd}}}$, as measured by the H1 experiment [89]. This function follows approximately an exponential of slope $-b_{\text{pd}}$, modified by the empirical parameter n_{pd} . Alternative models are discussed in Sec. 5. In addition, the PD contribution contains a nonresonant component which is modelled by an exponential shape in mass and the above-mentioned power-law model for p_T^2 . The parameters of the three power-laws are different for the J/ψ , $\psi(2S)$, and nonresonant dimuon components.

The parameters of the PD components are first determined by a fit to the control sample in each rapidity interval; an example fit is shown in Fig. 3. All parameters are free to vary in these fits except for the signal tail parameters, as explained above.

The PD models are then used as input in the fits to the signal sample. The p_T^2 shapes

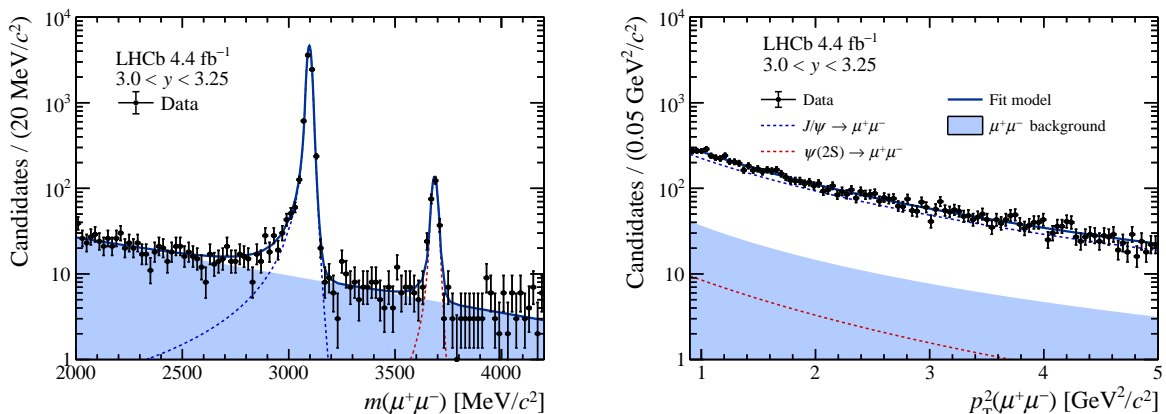


Figure 3: Distributions of (left) mass and (right) p_T^2 of data in the control sample for rapidity interval $3.0 < y < 3.25$. The fit described in the text is superimposed.

of the PD components are fixed to the values obtained on the corresponding control sample, while the PD J/ψ and $\psi(2S)$ mass shapes are forced to be identical to those of the CEP signals. The relative fractions of the two charmonia and the dimuon background are constrained from the fit to the control sample.

Exclusive continuum, or nonresonant dimuon production, is a QED process that takes place via the fusion of two photons. The dimuon pair produced in this form has low dimuon mass and a p_T^2 shape sharply peaked towards zero. The mass and p_T^2 distributions are correlated and therefore a two-dimensional histogram, which is obtained from simulation and validated with low- p_T^2 data, is used in the fit.

The J/ψ yield is affected by feed-down from higher-mass charmonium states, which is accounted for in the fit. The feed-down from $\psi(2S) \rightarrow J/\psi X$ decays is partially suppressed by the VELO and SPD multiplicity requirements. The yield of the remaining feed-down is determined from simulation of inclusive $\psi(2S) \rightarrow J/\psi X$ processes, normalised by the $\psi(2S)$ yield measured in each rapidity interval. Bin migration is taken into account via a migration matrix determined from simulation. An iterative procedure is applied to first determine the rapidity-dependent $\psi(2S)$ yield and then its contribution to the J/ψ yield. In practice, two steps are sufficient for the convergence of the procedure.

The normalisation of the feed-down from $\chi_c \rightarrow J/\psi\gamma$ decays is determined by reconstructing $J/\psi\gamma$ candidates in data. The same J/ψ selection as for CEP and PD candidates is used, except that the veto on additional photons is removed. Instead, photons with transverse energy in excess of 75 MeV are combined with J/ψ candidates to form χ_c candidates. In each y interval, where y is the rapidity of the J/ψ meson, and separately for the signal and control samples, the χ_{cJ} ($J = 0, 1, 2$) yields are determined from a fit to the resulting mass distribution. Fits to the χ_c samples are shown in Fig. 4. The three χ_{cJ} ($J = 0, 1, 2$) mass peaks are each modelled with a Crystal Ball function [84] with the tail parameters fixed from simulation. The peak of the Gaussian is free in the fit to account for imperfect photon energy calibration, but the shift with respect to the known masses of the χ_c mesons [85] is constrained to be the same for all three states. The shift varies between 6 and 10 MeV/ c^2 depending on the rapidity interval. The background is a mixture of partially reconstructed $\psi(2S)$ decays, such as $\psi(2S) \rightarrow J/\psi\pi^0\pi^0$, and random combinations of J/ψ mesons and calorimeter clusters. The same empirical function as in

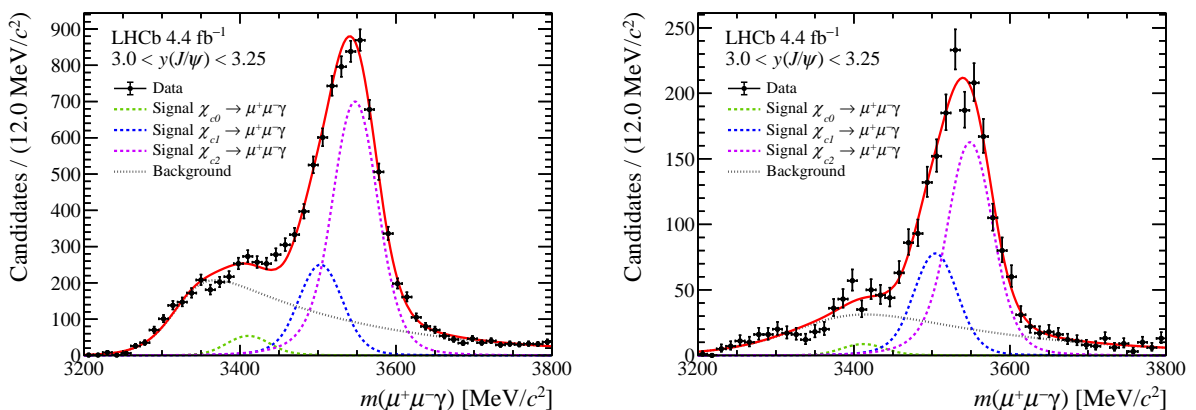


Figure 4: Fit to the $J/\psi\gamma$ mass distribution with the J/ψ meson in $3.0 < y < 3.25$ for (left) signal and (right) control samples.

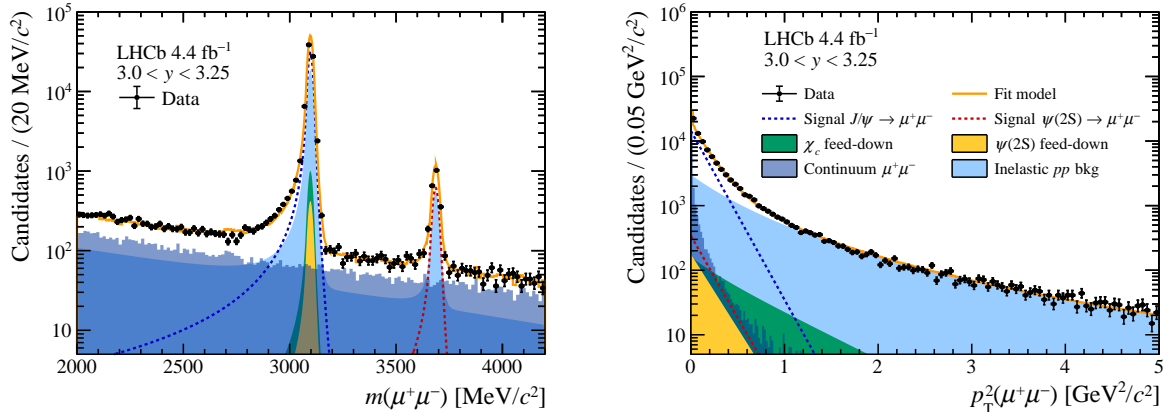


Figure 5: Distributions of (left) mass and (right) p_T^2 of data in the signal sample for the rapidity interval $3.0 < y < 3.25$. The fit described in the text is superimposed.

Ref. [90] is used as a model for the sum of these contributions.

The contribution from χ_{c0} mesons is small, while those of χ_{c1} and χ_{c2} mesons dominate. The empirical background model does not describe perfectly the mass distribution in the region below $3400 \text{ MeV}/c^2$, which has a negligible effect on the total χ_c yield. Due to the limited photon energy resolution, the mass fit has little sensitivity to the relative size of the χ_{c1} and χ_{c2} contributions. This ambiguity however does not affect the determination of the total J/ψ -from- $\chi_{c(1,2)}$ yield since (i) the branching fractions of the $\chi_{c(1,2)} \rightarrow J/\psi\gamma$ decays drop out in the ratio of J/ψ to $\chi_{c(1,2)}$ yields; (ii) the relative efficiencies for reconstructing $J/\psi\gamma$ and $J/\psi \rightarrow \mu^+\mu^-$ are equal for χ_{c1} and χ_{c2} , as determined from simulation; and (iii) the p_T^2 distributions of J/ψ from χ_{c1} and χ_{c2} are found to be equal in simulation and in data, which is checked by investigating the p_T^2 shape of candidates in the left and right halves of the $\chi_{c(1,2)}$ mass peak. The J/ψ -from- $\chi_{c(1,2)}$ yield is therefore proportional to the $\chi_{c(1,2)}$ yield in each rapidity interval. This feed-down contribution is determined in the signal and control samples, and the PD contribution is subtracted from that in CEP events to determine the overall CEP χ_c feed-down normalisation.

The J/ψ -from- $\psi(2S)$ and J/ψ -from- χ_c components are modelled in the CEP fit using the same mass model as for the J/ψ signal. The p_T^2 shapes are modelled with a single (double) exponential distribution for the $\psi(2S)$ (χ_c) feed-down, which is determined from simulation that is validated by data.

The mass and p_T^2 projections of the fit in the interval $3.0 < y < 3.25$ are shown in Fig. 5. All intervals are shown in Fig. 11 in Appendix C. The parameters of interest are the CEP J/ψ and $\psi(2S)$ yields, and the slopes of their p_T^2 shapes. In total, $299\,100 \pm 2100$ J/ψ and 7420 ± 130 $\psi(2S)$ elastically produced mesons are found in the fit to the full rapidity range.

4 Efficiencies

The signal yields are corrected for detection efficiencies using simulation samples calibrated with data, except for the HeRSChEL-related efficiencies, which are estimated in data.

A tag-and-probe method, aimed at measuring single-muon efficiencies, is applied to account for the differences between simulation and data. The simulation sample is then

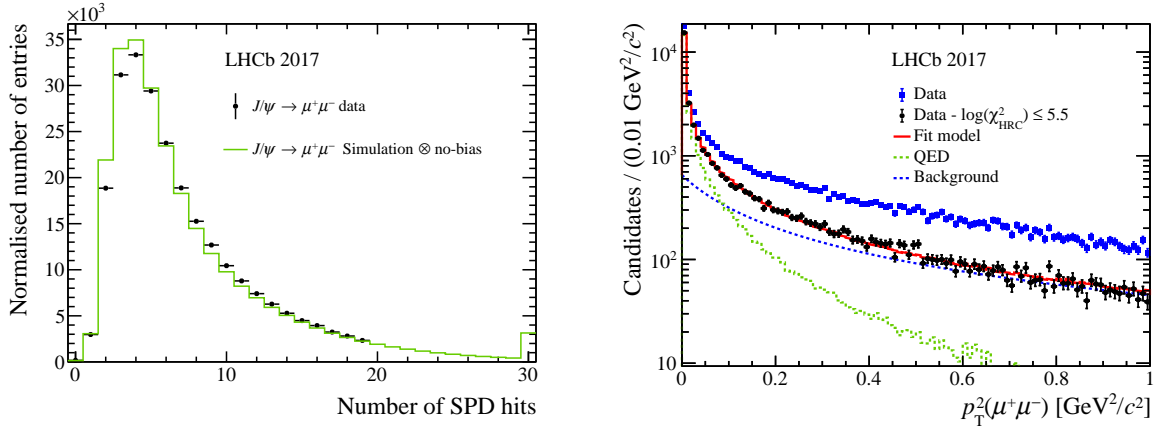


Figure 6: (Left) SPD multiplicity distributions in 2017 $J/\psi \rightarrow \mu^+ \mu^-$ data and modelling with simulation corrected using no-bias data from events with no beam crossing. The last bin contains the overflow events with 30 SPD hits or more. (Right) p_T^2 distributions in 2017 data without and with the HERSCHEL requirement applied. The fit is shown for the latter distribution.

weighted with the appropriate correction factors [66]. In this method, a tag muon from the J/ψ candidate is required to pass all selection criteria, while the other muon is used to measure the efficiency under investigation. The same procedure is applied to calibration samples and simulation, and the latter is weighted by the ratio of those efficiencies. The tracking, PID and hardware muon trigger efficiencies are calibrated in this manner. As most efficiencies depend on muon kinematics, they are determined in regions of muon pseudorapidity and transverse momentum, and separately for each year of data taking. Depending on the considered p_T, η region, correction factors range between 0.9 and 1.1 for tracking, 0.8 and 1.2 for PID, and 0.7 and 1.1 for muon trigger efficiencies, with uncertainties between 1% and 3%.

The hits in the SPD detector are due to charged particles reaching the detector, including those produced by the preshower detector, and to spill-over from the previous pp interaction. In the case of CEP events, which have only two muon tracks, the latter component dominates; however, it is not well modelled in simulation. The SPD hit distribution due to spill-over is obtained from data events that were collected by random triggers in unfilled bunch crossings that followed bunch crossings with a collision. This sample is referred to as no-bias data in the following. The obtained distribution is convolved with the SPD multiplicity in $J/\psi \rightarrow \mu^+ \mu^-$ simulation and matches reasonably well the distribution observed in CEP data, especially the tail up to the cut value of 20 SPD hits, as shown in Fig. 6. The fraction of events above this value defines the SPD trigger inefficiency, which is found to be independent of the dimuon kinematics.

The HERSCHEL detector is not included in the simulation. Its efficiency is determined using dimuon QED events, with and without the HERSCHEL vetoes applied. The p_T^2 distributions are shown in Fig. 6, emphasising the fact that the HERSCHEL requirement has little effect at low p_T^2 where QED backgrounds dominate. The efficiency is determined from the ratio of the QED components determined by the fits to the distributions with and without the HERSCHEL veto applied. It is found to be between 85% and 90% depending on data-taking period.

Efficiencies for the requirement on the absence of additional VELO tracks or photons

are taken from simulation and cross-checked in data in the same way as for the HERSCHEL veto efficiency. They are close to unity. The software trigger is fully efficient with respect to the offline selection. The total efficiency varies between 40% and 55%, with the lowest values being at the edges of the rapidity acceptance.

5 Systematic uncertainties

Systematic uncertainties arise due to the size of the simulation and calibration samples, and from the luminosity determination; they are mentioned in the sections above. Systematic uncertainties related to modelling choices are described below. All values are listed in Tables 1 and 2.

In the modelling of the number of SPD hits, N_{SPD} , the convolution of the no-bias data and the $J/\psi \rightarrow \mu^+\mu^-$ simulation is normalised to the distribution seen in data for $N_{\text{SPD}} < 20$. Alternatively, one could normalise it to get the best possible description of the tail, *i.e.* in the region $8 \leq N_{\text{SPD}} < 20$. The resulting change in SPD veto efficiency is reported as a systematic uncertainty.

The efficiencies of the HERSCHEL, track, and photon vetoes, collectively called global event cuts (GEC) in Table 1, are taken from the yield of QED events passing the veto. The fit models the non-QED background with the power-law from Ref. [89], but in this reduced p_{T}^2 region the sum of two exponential functions also provides a good description. The difference in measured efficiencies is taken as the associated systematic uncertainty.

The signal J/ψ and $\psi(2S)$ mass peaks are described by a modified Gaussian function. Other models, such as the sum of a Gaussian and a Crystal Ball function [84], are tried but yield poor-quality fits, without however significantly affecting the signal yields. No uncertainty is assigned. Similarly, the p_{T}^2 shape is modelled by a single exponential, as expected from theory, and there is no evidence of the need for another model.

The p_{T}^2 shapes of the J/ψ from feed-down are modelled with exponential functions taken from simulation. Alternatively, nonparametric distributions obtained from simulation are used, which yields a small change in the feed-down contributions and thus the signal yields. For the χ_c feed-down, a determination of the contribution from each χ_c state would be needed if their p_{T}^2 distributions were different. The present data do not require this. A dedicated CEP χ_c study using converted photons would be needed to resolve the χ_{c1} and χ_{c2} states.

The mass distribution of the inelastic pp background is described by the same shape as for the signal J/ψ and $\psi(2S)$ plus an exponential to describe the nonresonant dimuon contribution. A systematic uncertainty is estimated by changing the single exponential to the sum of two exponential functions.

Similarly, the p_{T}^2 shape for each component of the inelastic pp background is modelled with a power law. The sum of two exponentials also provides a reasonable fit, though of slightly lower quality. The systematic uncertainty due to this modelling is determined with pseudoexperiments. In each rapidity interval the data are fit with the alternate mass- p_{T}^2 model and then 500 pseudodata samples are generated using the fit result as model. These pseudosamples are then fit with the default model. The resulting biases of the J/ψ and $\psi(2S)$ yields are assigned as a systematic uncertainty.

Fit biases are tested in the same way. This time the default shape is used to generate 500 pseudodata samples which are fit with the same model. The variation of yields is

Table 1: Systematic and statistical uncertainties per rapidity interval for the J/ψ and $\psi(2S)$ cross-section in percent. The luminosity uncertainty is listed separately. Values below 0.005% are not shown.

Source / state	y bin	2.0–2.25		2.25–2.5		2.5–2.75		2.75–3.0		3.0–3.25	
		J/ψ	$\psi(2S)$	J/ψ	$\psi(2S)$	J/ψ	$\psi(2S)$	J/ψ	$\psi(2S)$	J/ψ	$\psi(2S)$
Uncorrelated uncertainties											
Simulation sample size		0.35	0.6	0.16	0.28	0.12	0.21	0.10	0.18	0.10	0.18
Bin migration		0.03	0.08		0.01			0.02	0.05	0.04	0.05
Muon efficiency		2.0	1.9	1.7	1.6	1.6	1.5	1.6	1.5	1.5	1.5
Mass: PD shape		0.06	0.22	0.01	0.17	0.10	0.22	0.10	0.18	0.19	0.33
p_T^2 : χ_c feed-down		0.01	0.01	0.01	0.06	0.03	0.01	0.04	0.01	0.02	0.03
p_T^2 : $\psi(2S)$ feed-down		0.12	0.04	0.01	0.09	0.01	0.02	0.02	0.02	0.03	0.04
p_T^2 : PD shape		3.5	1.8	0.20	0.4	0.30	0.11	0.01	0.7	0.32	1.2
Total uncorrelated		4.0	2.7	1.8	1.7	1.7	1.5	1.6	1.7	1.5	2.0
Correlated uncertainties											
GEC efficiency		0.8	0.8	0.8	0.8	0.8	0.8	0.8	0.8	0.8	0.8
GEC background		0.8	0.8	0.8	0.8	0.8	0.8	0.8	0.8	0.8	0.8
SPD hits efficiency		0.03	0.03	0.03	0.03	0.03	0.03	0.03	0.03	0.03	0.03
SPD multiplicity shape		0.15	0.15	0.15	0.15	0.15	0.15	0.15	0.15	0.15	0.15
Total correlated		1.2	1.2	1.2	1.2	1.2	1.2	1.2	1.2	1.2	1.2
Total uncertainties											
Systematic (excl. luminosity)		4.2	2.9	2.1	2.0	2.0	1.9	1.9	2.0	1.9	2.3
Luminosity		2.9	2.9	2.9	2.9	2.9	2.9	2.9	2.9	2.9	2.9
Statistical		2.3	12.6	1.5	6.1	1.1	4.6	1.0	4.1	0.9	4.0

Source / state	y bin	3.25–3.5		3.5–3.75		3.75–4.0		4.0–4.25		4.25–4.5	
		J/ψ	$\psi(2S)$	J/ψ	$\psi(2S)$	J/ψ	$\psi(2S)$	J/ψ	$\psi(2S)$	J/ψ	$\psi(2S)$
Uncorrelated uncertainties											
Simulation sample size		0.09	0.18	0.10	0.20	0.12	0.25	0.16	0.35	0.32	0.7
Bin migration		0.01	0.02	0.02	0.02		0.03	0.03	0.10	0.09	0.14
Muon efficiency		1.4	1.5	1.5	1.5	1.6	1.5	1.6	1.7	1.8	2.1
Mass: PD shape		0.17	0.28	0.13	0.15	0.13	0.32	0.06	0.20	0.03	0.10
p_T^2 : χ_c feed-down			0.01	0.02			0.03	0.03	0.03	0.03	0.02
p_T^2 : $\psi(2S)$ feed-down		0.04	0.01	0.01	0.02	0.01	0.04	0.05	0.01		0.04
p_T^2 : PD shape		0.6	0.6	0.8	1.6	1.0	2.1	1.5	2.2	1.5	0.9
Total uncorrelated		1.6	1.6	1.7	2.2	1.8	2.6	2.2	2.8	2.4	2.4
Correlated uncertainties											
GEC efficiency		0.8	0.8	0.8	0.8	0.8	0.8	0.8	0.8	0.8	0.8
GEC background		0.8	0.8	0.8	0.8	0.8	0.8	0.8	0.8	0.8	0.8
SPD hits efficiency		0.03	0.03	0.03	0.03	0.03	0.03	0.03	0.03	0.03	0.03
SPD multiplicity shape		0.15	0.15	0.15	0.15	0.15	0.15	0.15	0.15	0.15	0.15
Total correlated		1.2	1.2	1.2	1.2	1.2	1.2	1.2	1.2	1.2	1.2
Total uncertainties											
Systematic (excl. luminosity)		1.9	2.0	2.0	2.5	2.2	2.8	2.5	3.0	2.6	2.6
Luminosity		2.9	2.9	2.9	2.9	2.9	2.9	2.9	2.9	2.9	2.9
Statistical		0.9	3.6	1.0	4.3	1.2	5.2	1.6	7.7	2.5	16.2

Table 2: Systematic and statistical uncertainties per rapidity interval on the exponential slopes $b_{J/\psi}$ and $b_{\psi(2S)}$, in percent. Values below 0.005% are not reported.

y bin	2.0–2.25		2.25–2.5		2.5–2.75		2.75–3.0		3.0–3.25	
Source / state	J/ψ	$\psi(2S)$	J/ψ	$\psi(2S)$	J/ψ	$\psi(2S)$	J/ψ	$\psi(2S)$	J/ψ	$\psi(2S)$
Mass: PD	0.08	0.20	0.04	0.02	0.04	0.03	0.05	0.02	0.09	0.07
p_T^2 : χ_{cJ} feed-down	0.05	0.05	0.03		0.07		0.08	0.01	0.05	0.03
p_T^2 : $\psi(2S)$ feed-down	0.29	0.08	0.06				0.01	0.02	0.01	0.03
p_T^2 : PD shape	4.0	0.9	0.7	0.30	0.17	2.3	0.03	1.0	0.26	0.5
Total systematic	4.0	0.9	0.7	0.30	0.19	2.3	0.10	1.0	0.28	0.5
Statistical	2.6	14.4	1.5	8.0	1.2	5.6	1.0	5.2	0.9	5.0

y bin	3.25–3.5		3.5–3.75		3.75–4.0		4.0–4.25		4.25–4.5	
Source / state	J/ψ	$\psi(2S)$	J/ψ	$\psi(2S)$	J/ψ	$\psi(2S)$	J/ψ	$\psi(2S)$	J/ψ	$\psi(2S)$
Mass: PD	0.07	0.02	0.06	0.01	0.06	0.07	0.03		0.04	0.25
p_T^2 : χ_{cJ} feed-down	0.04	0.01	0.07	0.02	0.04		0.03	0.01	0.01	0.03
p_T^2 : $\psi(2S)$ feed-down	0.08		0.01	0.01	0.04		0.10	0.03	0.04	0.05
p_T^2 : PD shape	0.17	0.26	0.13	0.6	0.08	1.8	0.4	1.7	2.2	4.1
Total systematic	0.20	0.26	0.16	0.6	0.12	1.8	0.4	1.7	2.2	4.2
Statistical	0.9	4.6	1.0	5.4	1.2	6.3	1.7	9.9	2.9	20.4

compatible with the uncertainty returned from the fit, and the biases are negligible in comparison. No uncertainty is assigned.

Table 1 shows the values of all the systematic uncertainties previously discussed per rapidity interval for the $J/\psi \rightarrow \mu^+\mu^-$ and $\psi(2S) \rightarrow \mu^+\mu^-$ cross-section measurements. All uncertainties are assumed to be uncorrelated between rapidity intervals, except those for the SPD and HeRSChEL multiplicities, and for the luminosity, which are fully correlated.

The slope of the signal p_T^2 shape is only affected by changes in the fit model, leading to the systematic uncertainties listed in Table 2.

6 Results

The signal yields determined by the two-dimensional fit, the efficiencies and the resulting differential $pp \rightarrow pJ/\psi p$ and $pp \rightarrow p\psi(2S)p$ cross-sections are reported in Tables 4 and 5 in Appendix B. Summing over all rapidity intervals, the total integrated cross-sections for charmonia with $2.0 < y < 4.5$ and muons with $2.0 < \eta < 4.5$ are

$$\begin{aligned} \sigma_{J/\psi \rightarrow \mu^+\mu^-}(2.0 < y_{J/\psi} < 4.5, 2.0 < \eta_{\mu^\pm} < 4.5) &= 400 \pm 2 \pm 5 \pm 12 \text{ pb}, \\ \sigma_{\psi(2S) \rightarrow \mu^+\mu^-}(2.0 < y_{\psi(2S)} < 4.5, 2.0 < \eta_{\mu^\pm} < 4.5) &= 9.40 \pm 0.15 \pm 0.13 \pm 0.27 \text{ pb}, \end{aligned}$$

where the first uncertainties are statistical, the second systematic and the third are due to the luminosity determination. These values are more precise than those reported in the previous analysis of exclusive J/ψ and $\psi(2S)$ production at $\sqrt{s} = 13 \text{ TeV}$ [35] and are compatible at the level of 1.5σ .

The measured cross-sections are corrected for the $J/\psi \rightarrow \mu^+\mu^-$ and $\psi(2S) \rightarrow e^+e^-$ branching fractions [85] and the detector acceptance of the two muons, using simula-

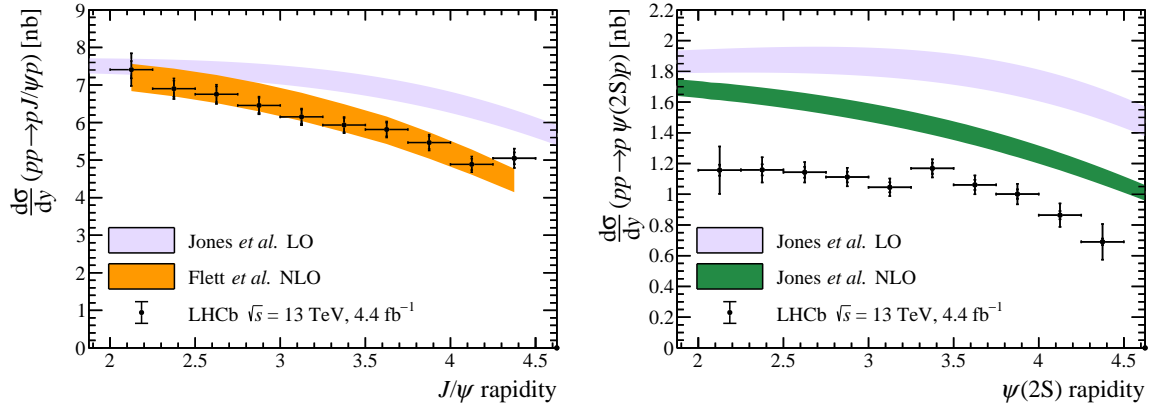


Figure 7: Differential cross-section for (left) J/ψ and (right) $\psi(2S)$ mesons. Theoretical predictions from Jones *et al.* [91, 92] and Flett *et al.* [45] are shown for comparison.

tion. The branching fraction for $\psi(2S) \rightarrow e^+e^-$ is used under the assumption of lepton universality as it is more precise than that of $\psi(2S) \rightarrow \mu^+\mu^-$. The resulting differential cross-sections are shown in Fig. 7. Theoretical predictions are shown for comparison. While the J/ψ cross-section agrees with the NLO prediction [45], which improves on the LO prediction [91], the $\psi(2S)$ cross-section is significantly lower than both the LO and NLO predictions [92]. The J/ψ cross-sections are used to determine the photoproduction cross-section as a function of the photon-proton energy, which is reported in Appendix A.

The ratio of $\psi(2S)$ and J/ψ cross-sections integrated over rapidity is found to be

$$\frac{\sigma_{\psi(2S)}}{\sigma_{J/\psi}} = 0.1763 \pm 0.0029 \pm 0.0008 \pm 0.0039,$$

where the last uncertainty is due to the knowledge of the branching fractions. The luminosity uncertainty cancels in the ratio. The ratio is shown in rapidity intervals in Fig. 8 and agrees with measurements by the LHCb collaboration in pp collisions at $\sqrt{s} = 7$ TeV [33] and PbPb collisions at $\sqrt{s_{NN}} = 5.02$ TeV [42]. Its average is consistent with those measured by the H1 and ZEUS collaborations [93, 94].

The photoproduction cross-section has an exponential behaviour versus p_T^2 : $d\sigma/dp_T^2 \sim e^{-bp_T^2}$. The exponential slope b can be parameterised as

$$b = b_0 + 4\alpha' \log \left(\frac{W_{\gamma p}}{W_0} \right), \quad (2)$$

where, in Regge theory, α' is the slope of the pomeron trajectory, $W_{\gamma p}$ is the photon-proton centre-of-mass energy defined in Appendix A, W_0 is typically taken to be $W_0 = 90$ GeV, and b_0 is determined experimentally.

A linear fit to the b slopes in intervals of rapidity is shown in Fig. 9. The intercepts

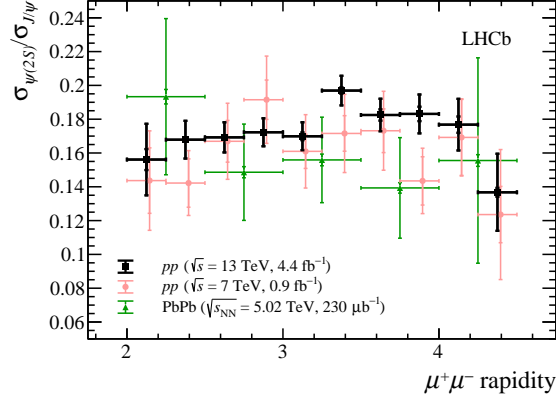


Figure 8: Measured ratio of $\psi(2S)$ and J/ψ cross-sections per rapidity interval. The results from PbPb collisions at $\sqrt{s_{NN}} = 5.02$ TeV [42] and pp collisions at $\sqrt{s} = 7$ TeV [33] are shown for comparison. The latter data points are slightly offset horizontally to increase visibility.

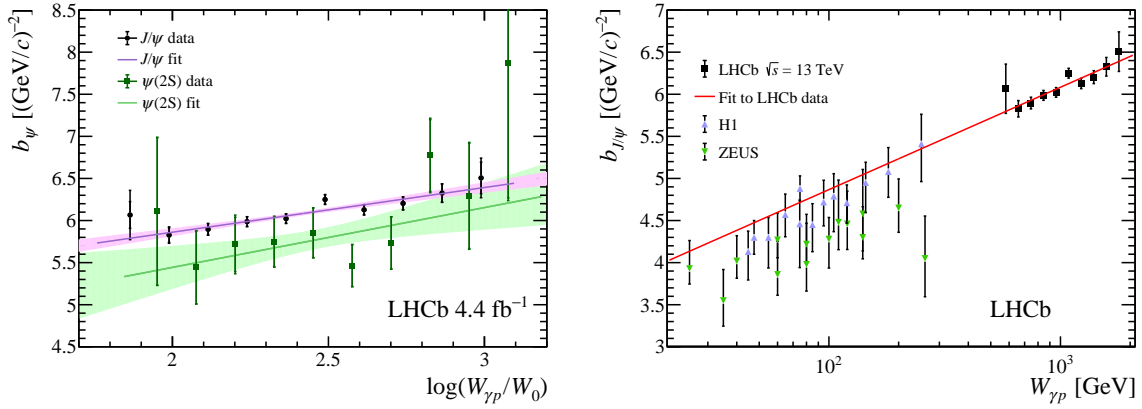


Figure 9: (Left) linear fit to the logarithmic dependence of $b_{J/\psi}$ and $b_{\psi(2S)}$ with respect to the photon-proton energy $W_{\gamma p}$ for J/ψ and $\psi(2S)$ production. The shaded areas represent the 68% C.L. fit uncertainties. (Right) measured b slopes for J/ψ production by the LHCb (this paper), H1 [89, 95] and ZEUS [96] experiments. Superimposed is a line with the slope resulting from the fit to the LHCb data.

and slopes are determined to be

$$\begin{aligned}\alpha'^{J/\psi} &= 0.133 \pm 0.024 \pm 0.006 \text{ (GeV}/c)^{-2}, \\ \alpha'^{\psi(2S)} &= 0.178 \pm 0.124 \pm 0.004 \text{ (GeV}/c)^{-2}, \\ b_0^{J/\psi} &= 4.80 \pm 0.24 \pm 0.06 \text{ (GeV}/c)^{-2}, \\ b_0^{\psi(2S)} &= 4.02 \pm 1.23 \pm 0.03 \text{ (GeV}/c)^{-2},\end{aligned}$$

where the first uncertainty is statistical and the second systematic. The systematic uncertainties are obtained by taking the difference of the central value when the fit is performed with and without the systematic uncertainties accounted for in the fit. The fit to J/ψ data agrees with previous determinations in ep collisions [89, 95–97] but is below the prediction of Ref. [98].

7 Conclusion

This paper presents the first measurement of the exclusive $\psi(2S)$ cross-section in pp collisions at $\sqrt{s} = 13$ TeV in ten intervals of rapidity between 2.0 and 4.5. The corresponding J/ψ cross-section is updated and their rapidity-dependent ratio is determined for the first time. The results are consistent but more precise than those of Ref. [35]. When expressed as a function of the photon-proton energy, the cross-sections are found to be consistent with previous measurements, but the $\psi(2S)$ cross-section is below theory predictions.

For the first time, the dependence of the J/ψ and $\psi(2S)$ cross-sections on $p_{\text{T}}^2 \sim \Delta t$, where Δt is the total transverse momentum transfer, is determined in pp collisions and is found consistent with the behaviour observed at HERA [89, 95–97].

Acknowledgements

We express our gratitude to our colleagues in the CERN accelerator departments for the excellent performance of the LHC. We thank the technical and administrative staff at the LHCb institutes. We acknowledge support from CERN and from the national agencies: CAPES, CNPq, FAPERJ and FINEP (Brazil); MOST and NSFC (China); CNRS/IN2P3 (France); BMBF, DFG and MPG (Germany); INFN (Italy); NWO (Netherlands); MNiSW and NCN (Poland); MCID/IFA (Romania); MICIU and AEI (Spain); SNSF and SER (Switzerland); NASU (Ukraine); STFC (United Kingdom); DOE NP and NSF (USA). We acknowledge the computing resources that are provided by CERN, IN2P3 (France), KIT and DESY (Germany), INFN (Italy), SURF (Netherlands), PIC (Spain), GridPP (United Kingdom), CSCS (Switzerland), IFIN-HH (Romania), CBPF (Brazil), and Polish WLCG (Poland). We are indebted to the communities behind the multiple open-source software packages on which we depend. Individual groups or members have received support from ARC and ARDC (Australia); Key Research Program of Frontier Sciences of CAS, CAS PIFI, CAS CCEPP, Fundamental Research Funds for the Central Universities, and Sci. & Tech. Program of Guangzhou (China); Minciencias (Colombia); EPLANET, Marie Skłodowska-Curie Actions, ERC and NextGenerationEU (European Union); A*MIDEX, ANR, IPhU and Labex P2IO, and Région Auvergne-Rhône-Alpes (France); AvH Foundation (Germany); ICSC (Italy); Severo Ochoa and María de Maeztu Units of Excellence, GVA, XuntaGal, GENCAT, InTalent-Inditex and Prog. Atracción Talento CM (Spain); SRC (Sweden); the Leverhulme Trust, the Royal Society and UKRI (United Kingdom).

Appendices

A Photoproduction cross-section

The differential cross-sections are used to determine the photoproduction cross-section for J/ψ and $\psi(2S)$ mesons. The differential cross-section is factorised into two terms depending on whether the proton travelling from the vertex detector towards the muon chambers interacts electromagnetically (labelled $W_{\gamma p,+}$) or the opposite-direction proton does (labelled $W_{\gamma p,-}$):

$$\frac{d\sigma}{dy}(pp \rightarrow p\psi p) = S^2(W_{\gamma p,+}) \left(k_+ \frac{dn}{dk_+} \right) \sigma_{\gamma p \rightarrow \psi p}^{W_{\gamma p,+}} + S^2(W_{\gamma p,-}) \left(k_- \frac{dn}{dk_-} \right) \sigma_{\gamma p \rightarrow \psi p}^{W_{\gamma p,-}}, \quad (3)$$

with $W_{\gamma p,\pm} = \sqrt{M_\psi c^2 \sqrt{s} e^{\pm|y|}}$. The $S^2(W_{\gamma p,\pm})$ terms, the so-called survival factors, are taken from Ref. [99]. The photon flux dn/dk_\pm for photons with energy equal to $k_\pm = (M_\psi c^2/2)e^{\pm|y|}$ is calculated following Refs. [100, 101]. The photoproduction cross-sections are given by $\sigma_{\gamma p \rightarrow \psi p}^{W_{\gamma p,\pm}}$. The antiparallel γp cross-section, $\sigma_{\gamma p \rightarrow \psi p}^{W_{\gamma p,-}}$, corresponds to large values of x , as $x \sim M_\psi c^2 / \sqrt{s} e^{-y}$ [45]. The contribution of this term to Eq. 3 is therefore expected to be small and can be constrained from theoretical predictions. The antiparallel solution is taken from the J/ψ and $\psi(2S)$ NLO cross-section predictions from Refs. [45, 92] and subtracted. Figure 10 shows the measured photoproduction cross-section for J/ψ mesons and compares it with previous measurements listed in Table 3. The numerical values are listed in Table 8.

The LHCb J/ψ data at $\sqrt{s} = 13$ TeV are in agreement with the NLO description [45]. They also follow a power-law fit to H1 data [89].

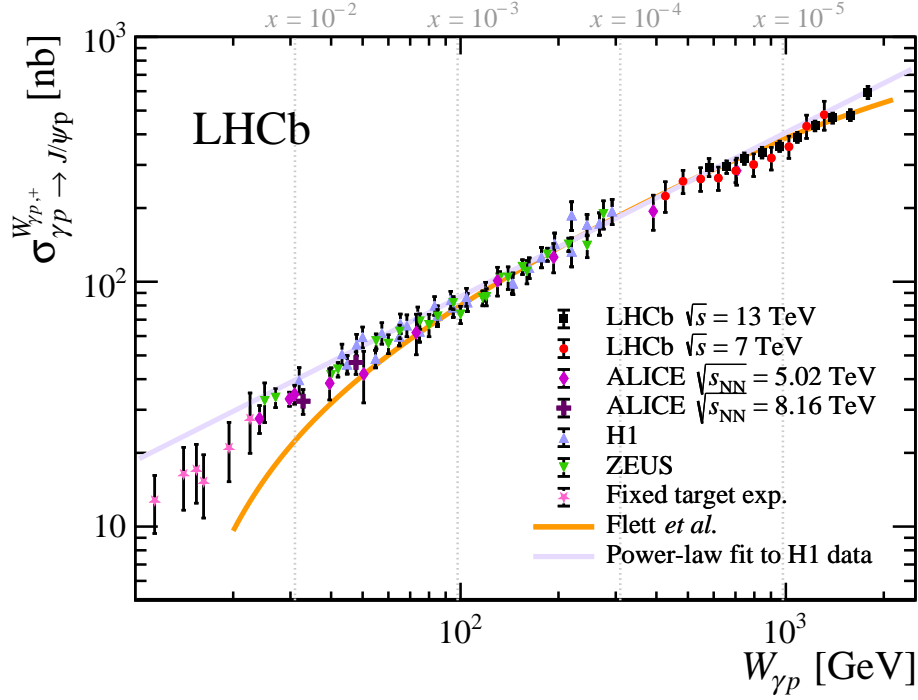


Figure 10: Results for the J/ψ photoproduction cross-section as a function of the photon-proton energy $W_{\gamma p}$ from different experiments listed in Table 3. The LHCb results at $\sqrt{s} = 13$ TeV are estimated with the NLO [45] calculation. Also shown are the NLO theoretical descriptions given by Flett *et al.* [45], as well as a power-law description of the H1 data. The top axis shows the values of x reached for a given photon-proton energy.

Table 3: Previous results used in Fig. 10.

Marker	Experiment	collision	Energy	Refs.
●	LHCb	pp	$\sqrt{s} = 7$ TeV	[33]
◆	ALICE	pPb	$\sqrt{s_{NN}} = 5.02$ TeV	[102, 103]
+	ALICE	pPb	$\sqrt{s_{NN}} = 8.16$ TeV	[39]
▲	H1	ep	$40 < W_{\gamma p} < 305$ GeV	[95]
▲	H1	ep	$25 < W_{\gamma p} < 110$ GeV	[89]
▼	ZEUS	ep	$20 < W_{\gamma p} < 290$ GeV	[96]
*	E87	γBe	$0 < E_{\gamma} < 250$ GeV	[104]
*	E401	γH and $\gamma^2 H$	$60 < E_{\gamma} < 300$ GeV	[105]
*	E516	γH	$60 < E_{\gamma} < 160$ GeV	[106]

B Numerical results

Tables 4 and 5 present the differential cross-sections in rapidity bins, shown in Fig. 7, and the breakdown of uncertainties for $J/\psi \rightarrow \mu^+\mu^-$ and $\psi(2S) \rightarrow \mu^+\mu^-$, respectively. Their ratio is given in Table 6. Table 7 lists the exponential slopes for J/ψ and $\psi(2S)$ in each rapidity bin, corresponding to Fig. 9. Table 8 lists the values entering the computation of the parallel cross-sections $\sigma_{\gamma p \rightarrow J/\psi p}^{W_{\gamma p, +}}$ displayed in Fig. 10.

Table 4: Differential CEP $J/\psi \rightarrow \mu^+\mu^-$ yields and cross-sections corrected for efficiency (ϵ_{tot}), acceptance ($\epsilon_{\text{Geom.Acc.}}$) and branching fraction. The systematic uncertainties are split between those uncorrelated across y ranges, those that are 100% correlated and the luminosity uncertainty.

$y_{J/\psi}$ bin	2.0–2.25	2.25–2.5	2.5–2.75	2.75–3.0	3.0–3.25
N_{sig}	4998 ± 113	18095 ± 265	31591 ± 361	41640 ± 402	47690 ± 432
ϵ_{tot}	0.313 ± 0.028	0.403 ± 0.030	0.443 ± 0.030	0.456 ± 0.029	0.467 ± 0.027
$\epsilon_{\text{Geom.Acc.}}$	0.095 ± 0.002	0.287 ± 0.003	0.466 ± 0.003	0.623 ± 0.003	0.732 ± 0.003
$d\sigma/dy$ [nb]	7.41	6.90	6.75	6.46	6.15
Stat. unc. [nb]	0.17	0.10	0.08	0.06	0.06
Uncorr. syst. unc. [nb]	0.30	0.12	0.11	0.10	0.09
Corr. syst. unc. [nb]	0.23	0.21	0.21	0.20	0.19
Lumi. unc. [nb]	0.21	0.20	0.20	0.19	0.18
$y_{J/\psi}$ bin	3.25–3.5	3.5–3.75	3.75–4.0	4.0–4.25	4.25–4.5
N_{sig}	47303 ± 436	39878 ± 394	26727 ± 329	14428 ± 236	4349 ± 108
ϵ_{tot}	0.479 ± 0.027	0.484 ± 0.028	0.462 ± 0.029	0.435 ± 0.029	0.399 ± 0.029
$\epsilon_{\text{Geom.Acc.}}$	0.733 ± 0.003	0.625 ± 0.003	0.467 ± 0.003	0.300 ± 0.003	0.095 ± 0.002
$d\sigma/dy$ [nb]	5.93	5.82	5.47	4.89	5.05
Stat. unc. [nb]	0.05	0.06	0.07	0.08	0.13
Uncorr. syst. unc. [nb]	0.09	0.10	0.10	0.11	0.12
Corr. syst. unc. [nb]	0.18	0.18	0.17	0.15	0.16
Lumi. unc. [nb]	0.17	0.17	0.16	0.14	0.15

Table 5: Differential CEP $\psi(2S) \rightarrow \mu^+\mu^-$ yields and cross-sections corrected for efficiency (ϵ_{tot}), acceptance ($\epsilon_{\text{Geom.Acc.}}$) and branching fraction. The systematic uncertainties are split between those uncorrelated across y ranges, those that are 100% correlated and the luminosity uncertainty.

$y_{\psi(2S)}$ bin	2.0–2.25	2.25–2.5	2.5–2.75	2.75–3.0	3.0–3.25
N_{sig}	127 ± 16	491 ± 30	845 ± 39	1088 ± 44	1163 ± 47
ϵ_{tot}	0.400 ± 0.032	0.494 ± 0.032	0.527 ± 0.032	0.518 ± 0.032	0.502 ± 0.031
$\epsilon_{\text{Geom.Acc.}}$	0.091 ± 0.002	0.284 ± 0.003	0.465 ± 0.003	0.626 ± 0.003	0.735 ± 0.003
$d\sigma/dy$ [nb]	1.16	1.16	1.14	1.11	1.05
Stat. unc. [nb]	0.15	0.07	0.05	0.05	0.04
Uncorr. syst. unc. [nb]	0.03	0.02	0.02	0.02	0.02
Corr. syst. unc. [nb]	0.04	0.04	0.04	0.03	0.03
Lumi. unc. [nb]	0.03	0.03	0.03	0.03	0.03
$y_{\psi(2S)}$ bin	3.25–3.5	3.5–3.75	3.75–4.0	4.0–4.25	4.25–4.5
N_{sig}	1319 ± 48	980 ± 42	648 ± 34	323 ± 25	81 ± 13
ϵ_{tot}	0.505 ± 0.030	0.492 ± 0.030	0.457 ± 0.030	0.427 ± 0.030	0.394 ± 0.035
$\epsilon_{\text{Geom.Acc.}}$	0.740 ± 0.003	0.622 ± 0.003	0.469 ± 0.003	0.290 ± 0.003	0.099 ± 0.002
$d\sigma/dy$ [nb]	1.17	1.06	1.00	0.86	0.69
Stat. unc. [nb]	0.04	0.05	0.05	0.07	0.11
Uncorr. syst. unc. [nb]	0.02	0.02	0.03	0.02	0.02
Corr. syst. unc. [nb]	0.04	0.03	0.03	0.03	0.02
Lumi. unc. [nb]	0.03	0.03	0.03	0.02	0.02

Table 6: Ratio of the CEP $J/\psi \rightarrow \mu^+\mu^-$ and $\psi(2S) \rightarrow \mu^+\mu^-$ cross-sections per rapidity bin.

y bin	2.0–2.25	2.25–2.5	2.5–2.75	2.75–3.0	3.0–3.25
$\frac{d\sigma_{\psi(2S)}/dy}{d\sigma_{J/\psi}/dy}$	0.156	0.168	0.169	0.172	0.170
Stat. unc.	0.020	0.010	0.008	0.007	0.007
Syst. unc.	0.006	0.001	0.001	0.001	0.002
BF unc.	0.003	0.004	0.004	0.004	0.004
y bin	3.25–3.5	3.5–3.75	3.75–4.0	4.0–4.25	4.25–4.5
$\frac{d\sigma_{\psi(2S)}/dy}{d\sigma_{J/\psi}/dy}$	0.197	0.182	0.183	0.177	0.137
Stat. unc.	0.007	0.008	0.010	0.014	0.022
Syst. unc.	0.002	0.003	0.004	0.005	0.003
BF unc.	0.004	0.004	0.004	0.004	0.003

Table 7: Values of the b slopes measured in the fit.

y	$\log\left(\frac{W_{\gamma p}^{J/\psi}}{W_0}\right)$	$b^{J/\psi}$	$\log\left(\frac{W_{\gamma p}^{\psi(2S)}}{W_0}\right)$	$b^{\psi(2S)}$
2.0–2.25	1.86	$6.07 \pm 0.16 \pm 0.25$	1.95	$6.1 \pm 0.9 \pm 0.1$
2.25–2.5	1.99	$5.83 \pm 0.09 \pm 0.04$	2.08	$5.4 \pm 0.4 \pm 0.0$
2.5–2.75	2.11	$5.90 \pm 0.07 \pm 0.01$	2.20	$5.7 \pm 0.3 \pm 0.1$
2.75–3.0	2.24	$5.99 \pm 0.06 \pm 0.01$	2.33	$5.7 \pm 0.3 \pm 0.1$
3.0–3.25	2.36	$6.02 \pm 0.05 \pm 0.02$	2.45	$5.9 \pm 0.3 \pm 0.0$
3.25–3.5	2.49	$6.25 \pm 0.06 \pm 0.01$	2.58	$5.5 \pm 0.2 \pm 0.0$
3.5–3.75	2.61	$6.13 \pm 0.06 \pm 0.01$	2.70	$5.7 \pm 0.3 \pm 0.0$
3.75–4.0	2.74	$6.20 \pm 0.08 \pm 0.01$	2.83	$6.8 \pm 0.4 \pm 0.1$
4.0–4.25	2.86	$6.33 \pm 0.11 \pm 0.02$	2.95	$6.3 \pm 0.6 \pm 0.1$
4.25–4.5	2.99	$6.51 \pm 0.19 \pm 0.14$	3.08	$7.9 \pm 1.6 \pm 0.3$

 Table 8: Values of the differential cross-section, survival factor, photon flux and antiparallel photoproduction cross-section used for the calculation of the parallel cross-section. The antiparallel γp value is taken from the FMRT NLO description [45].

$y_{J/\psi}$ bin	2.0–2.25	2.25–2.5	2.5–2.75	2.75–3.0	3.0–3.25
$d\sigma/dy$ [nb]	7.41 ± 0.43	6.90 ± 0.27	6.75 ± 0.25	6.46 ± 0.24	6.15 ± 0.22
$S^2(W_{\gamma p,+})$	0.786	0.774	0.762	0.748	0.732
$k_+ \frac{dn}{dk_+} (\times 10^{-3})$	22.7	21.6	20.4	19.2	18.0
$S^2(W_{\gamma p,-})$	0.885	0.888	0.891	0.893	0.896
$k_- \frac{dn}{dk_-} (\times 10^{-3})$	42.5	43.7	44.9	46.0	47.2
$\sigma_{\gamma p \rightarrow J/\psi p}^{W_{\gamma p,-}}$ [nb]	57.7 ± 2.7	51.1 ± 2.3	45.0 ± 2.0	39.2 ± 1.7	33.9 ± 1.4
$\sigma_{\gamma p \rightarrow J/\psi p}^{W_{\gamma p,+}}$ [nb]	294 ± 25	294 ± 17	319 ± 17	337 ± 17	358 ± 17
$y_{J/\psi}$ bin	3.25–3.5	3.5–3.75	3.75–4.0	4.0–4.25	4.25–4.5
$d\sigma/dy$ [nb]	5.93 ± 0.21	5.82 ± 0.21	5.47 ± 0.21	4.89 ± 0.21	5.05 ± 0.26
$S^2(W_{\gamma p,+})$	0.715	0.695	0.672	0.647	0.618
$k_+ \frac{dn}{dk_+} (\times 10^{-3})$	16.8	21.6	14.5	13.3	12.1
$S^2(W_{\gamma p,-})$	0.899	0.901	0.903	0.905	0.907
$k_- \frac{dn}{dk_-} (\times 10^{-3})$	48.3	49.5	50.7	51.8	53.0
$\sigma_{\gamma p \rightarrow J/\psi p}^{W_{\gamma p,-}}$ [nb]	29.0 ± 1.2	24.4 ± 0.9	20.1 ± 0.7	16.2 ± 0.6	12.6 ± 0.4
$\sigma_{\gamma p \rightarrow J/\psi p}^{W_{\gamma p,+}}$ [nb]	389 ± 18	433 ± 20	467 ± 22	480 ± 25	594 ± 34

C Fits in all rapidity bins

The distributions of dimuon mass and p_T^2 in each rapidity interval are shown in Fig. 11. The results of the two-dimensional fits described in the main text are overlaid.

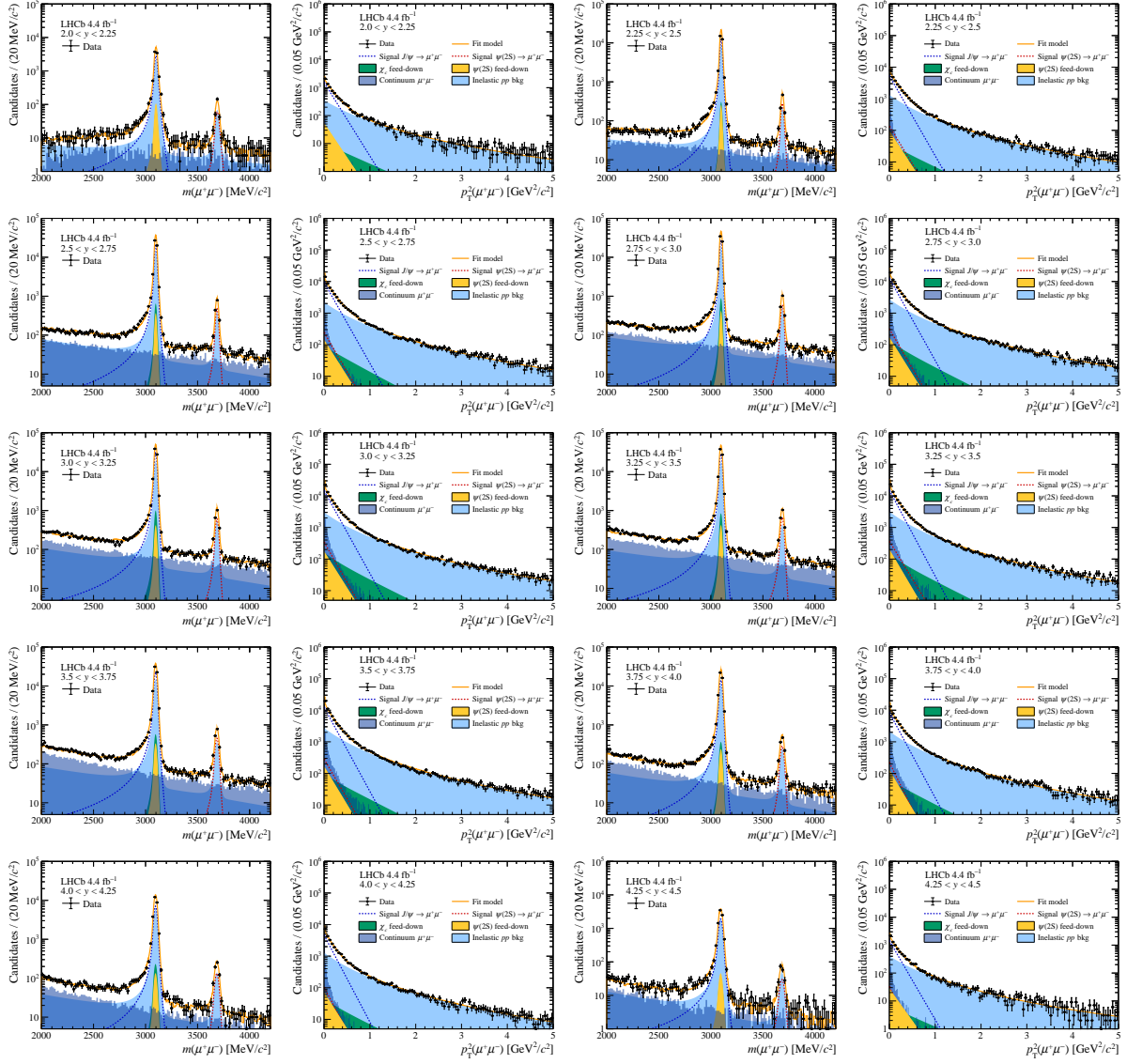


Figure 11: Distributions of dimuon mass and p_T^2 for the CEP sample in different regions of rapidity. The results of the two-dimensional fits are overlaid.

References

- [1] E. D. Bloom *et al.*, *High-energy inelastic ep scattering at 6-degrees and 10-degrees*, *Phys. Rev. Lett.* **23** (1969) 930.
- [2] M. Breidenbach *et al.*, *Observed behavior of highly inelastic electron-proton scattering*, *Phys. Rev. Lett.* **23** (1969) 935.
- [3] T.-J. Hou *et al.*, *New CTEQ global analysis of quantum chromodynamics with high-precision data from the LHC*, *Phys. Rev.* **D103** (2021) 014013, [arXiv:1912.10053](#).
- [4] NNPDF collaboration, R. D. Ball *et al.*, *Parton distributions from high-precision collider data*, *Eur. Phys. J.* **C77** (2017) 663, [arXiv:1706.00428](#).
- [5] S. Bailey *et al.*, *Parton distributions from LHC, HERA, Tevatron and fixed target data: MSHT20 PDFs*, *Eur. Phys. J.* **C81** (2021) 341, [arXiv:2012.04684](#).
- [6] H1, ZEUS collaboration, H. Abramowicz *et al.*, *Combination of measurements of inclusive deep inelastic e^+p scattering cross sections and QCD analysis of HERA data*, *Eur. Phys. J.* **C75** (2015) 580, [arXiv:1506.06042](#).
- [7] H1 and ZEUS collaborations, H. Abramowicz *et al.*, *Combination and QCD analysis of charm and beauty production cross-section measurements in deep inelastic ep scattering at HERA*, *Eur. Phys. J.* **C78** (2018) 473, [arXiv:1804.01019](#).
- [8] LHCb collaboration, R. Aaij *et al.*, *Measurement of the forward Z boson cross-section in pp collisions at $\sqrt{s} = 7$ TeV*, *JHEP* **08** (2015) 039, [arXiv:1505.07024](#).
- [9] LHCb collaboration, R. Aaij *et al.*, *Measurement of $Z \rightarrow e^+e^-$ production at $\sqrt{s} = 8$ TeV*, *JHEP* **05** (2015) 109, [arXiv:1503.00963](#).
- [10] LHCb collaboration, R. Aaij *et al.*, *Measurement of forward W and Z boson production in pp collisions at $\sqrt{s} = 8$ TeV*, *JHEP* **01** (2016) 155, [arXiv:1511.08039](#).
- [11] LHCb collaboration, R. Aaij *et al.*, *Inclusive W and Z production in the forward region at $\sqrt{s} = 7$ TeV*, *JHEP* **06** (2012) 058, [arXiv:1204.1620](#).
- [12] LHCb collaboration, R. Aaij *et al.*, *Measurements of prompt charm production cross-sections in pp collisions at $\sqrt{s} = 13$ TeV*, *JHEP* **03** (2016) 159, Erratum *ibid.* **09** (2016) 013, Erratum *ibid.* **05** (2017) 074, [arXiv:1510.01707](#).
- [13] R. Gauld and J. Rojo, *Precision determination of the small-x gluon from charm production at LHCb*, *Phys. Rev. Lett.* **118** (2017) 072001, [arXiv:1610.09373](#).
- [14] PROSA collaboration, O. Zenaiev *et al.*, *Impact of heavy-flavour production cross sections measured by the LHCb experiment on parton distribution functions at low x*, *Eur. Phys. J.* **C75** (2015) 396, [arXiv:1503.04581](#).
- [15] V. Bertone, R. Gauld, and J. Rojo, *Neutrino telescopes as QCD microscopes*, *JHEP* **01** (2019) 217, [arXiv:1808.02034](#).

- [16] C. A. Flett, A. D. Martin, M. G. Ryskin, and T. Teubner, *Implications of exclusive J/ψ photoproduction in a tamed collinear factorisation approach to NLO*, *SciPost Phys. Proc.* **15** (2024) 005, [arXiv:2209.15277](#).
- [17] M. G. Ryskin, *Diffractive J/ψ electroproduction in LLA QCD*, *Z. Phys.* **C57** (1993) 89.
- [18] H. Mäntysaari and J. Penttala, *Complete calculation of exclusive heavy vector meson production at next-to-leading order in the dipole picture*, *JHEP* **08** (2022) 247, [arXiv:2204.14031](#).
- [19] C. A. Flett *et al.*, *How to include exclusive J/ψ production data in global PDF analyses*, *Phys. Rev.* **D101** (2020) 094011, [arXiv:1908.08398](#).
- [20] M. Diehl, *Generalized parton distributions*, *Phys. Rept.* **388** (2003) 41, [arXiv:hep-ph/0307382](#).
- [21] S. R. Klein and H. Mäntysaari, *Imaging the nucleus with high-energy photons*, *Nature Rev. Phys.* **1** (2019) 662, [arXiv:1910.10858](#).
- [22] J. Nemchik *et al.*, *The diffraction cone for exclusive vector meson production in deep inelastic scattering*, *J. Exp. Theor. Phys.* **86** (1998) 1054, [arXiv:hep-ph/9712469](#).
- [23] J. Nemchik, *Wave function of $2S$ radially excited vector mesons from data for diffraction slope*, *Phys. Rev.* **D63** (2001) 074007, [arXiv:hep-ph/0003245](#).
- [24] M. Hentschinski and E. Padrón Molina, *Exclusive J/ψ and $\psi(2S)$ photo-production as a probe of QCD low x evolution equations*, *Phys. Rev.* **D103** (2021) 074008, [arXiv:2011.02640](#).
- [25] J. Hufner, Y. P. Ivanov, B. Z. Kopeliovich, and A. V. Tarasov, *Photoproduction of charmonia and total charmonium proton cross-sections*, *Phys. Rev.* **D62** (2000) 094022, [arXiv:hep-ph/0007111](#).
- [26] B. Z. Kopeliovich and B. G. Zakharov, *Quantum effects and color transparency in charmonium photoproduction on nuclei*, *Phys. Rev.* **D44** (1991) 3466.
- [27] B. Z. Kopeliovich, J. Nemchik, N. N. Nikolaev, and B. G. Zakharov, *Decisive test of color transparency in exclusive electroproduction of vector mesons*, *Phys. Lett.* **B324** (1994) 469, [arXiv:hep-ph/9311237](#).
- [28] J. Nemchik, N. N. Nikolaev, and B. G. Zakharov, *Scanning the BFKL pomeron in elastic production of vector mesons at HERA*, *Phys. Lett.* **B341** (1994) 228, [arXiv:hep-ph/9405355](#).
- [29] N. Armesto and A. H. Rezaeian, *Exclusive vector meson production at high energies and gluon saturation*, *Phys. Rev.* **D90** (2014) 054003, [arXiv:1402.4831](#).
- [30] T. Lappi and H. Mäntysaari, *Incoherent diffractive J/ψ -production in high energy nuclear DIS*, *Phys. Rev.* **C83** (2011) 065202, [arXiv:1011.1988](#).

- [31] H. Kowalski, L. Motyka, and G. Watt, *Exclusive diffractive processes at HERA within the dipole picture*, *Phys. Rev.* **D74** (2006) 074016, [arXiv:hep-ph/0606272](#).
- [32] LHCb collaboration, R. Aaij *et al.*, *Exclusive J/ψ and $\psi(2S)$ production in pp collisions at $\sqrt{s} = 7$ TeV*, *J. Phys.* **G40** (2013) 045001, [arXiv:1301.7084](#).
- [33] LHCb collaboration, R. Aaij *et al.*, *Updated measurements of exclusive J/ψ and $\psi(2S)$ production cross-sections in pp collisions at $\sqrt{s} = 7$ TeV*, *J. Phys.* **G41** (2014) 055002, [arXiv:1401.3288](#).
- [34] CMS collaboration, A. Tumasyan *et al.*, *Probing small Bjorken- x nuclear gluonic structure via coherent J/ψ photoproduction in ultraperipheral Pb-Pb collisions at $\sqrt{s_{NN}} = 5.02$ TeV*, *Phys. Rev. Lett.* **131** (2023) 262301, [arXiv:2303.16984](#).
- [35] LHCb collaboration, R. Aaij *et al.*, *Central exclusive production of J/ψ and $\psi(2S)$ mesons in pp collisions at $\sqrt{s} = 13$ TeV*, *JHEP* **10** (2018) 167, [arXiv:1806.04079](#).
- [36] LHCb collaboration, R. Aaij *et al.*, *Observation of charmonium pairs produced exclusively in pp collisions*, *J. Phys.* **G41** (2014) 115002, [arXiv:1407.5973](#).
- [37] LHCb collaboration, R. Aaij *et al.*, *Measurement of the exclusive $\Upsilon(nS)$ production cross-section in pp collisions at $\sqrt{s} = 7$ TeV and 8 TeV*, *JHEP* **09** (2015) 084, [arXiv:1505.08139](#).
- [38] LHCb collaboration, R. Aaij *et al.*, *Observation of exotic $J/\psi\phi$ resonances in diffractive processes in proton-proton collisions*, [arXiv:2407.14301](#), Submitted to *Phys. Rev. Lett.*
- [39] ALICE collaboration, S. Acharya *et al.*, *Exclusive and dissociative J/ψ photoproduction, and exclusive dimuon production, in p -Pb collisions at $\sqrt{s_{NN}} = 8.16$ TeV*, *Phys. Rev.* **D108** (2023) 112004, [arXiv:2304.12403](#).
- [40] ALICE collaboration, S. Acharya *et al.*, *Coherent J/ψ photoproduction at forward rapidity in ultra-peripheral Pb-Pb collisions at $\sqrt{s_{NN}} = 5.02$ TeV*, *Phys. Lett.* **B798** (2019) 134926, [arXiv:1904.06272](#).
- [41] ALICE collaboration, *First polarisation measurement of coherently photoproduced J/ψ in ultra-peripheral Pb-Pb collisions at $\sqrt{s_{NN}} = 5.02$ TeV*, [arXiv:2304.10928](#).
- [42] LHCb collaboration, R. Aaij *et al.*, *Study of exclusive photoproduction of charmonium in ultra-peripheral lead-lead collisions*, *JHEP* **06** (2023) 146, [arXiv:2206.08221](#).
- [43] D. Boer and C. Setyadi, *Probing gluon GTMDs through exclusive coherent diffractive processes*, *Eur. Phys. J.* **C83** (2023) 890, [arXiv:2301.07980](#).
- [44] C. A. Flett *et al.*, *Predictions of exclusive Υ photoproduction at the LHC and future colliders*, *Phys. Rev.* **D105** (2022) 034008, [arXiv:2110.15575](#).
- [45] C. A. Flett, A. D. Martin, M. G. Ryskin, and T. Teubner, *Very low x gluon density determined by LHCb exclusive J/ψ data*, *Phys. Rev.* **D102** (2020) 114021, [arXiv:2006.13857](#).

- [46] N. Sharma, *Exclusive diffractive J/ψ and $\psi(2S)$ production in dipole model using a holographic AdS/QCD light-front wavefunction with longitudinal confinement*, *Phys. Rev. D* **D109** (2024) 014019, [arXiv:2311.09152](#).
- [47] H. Mäntysaari, F. Salazar, and B. Schenke, *Energy dependent nuclear suppression from gluon saturation in exclusive vector meson production*, *Phys. Rev. D* **D109** (2024) L071504, [arXiv:2312.04194](#).
- [48] H. Mäntysaari, F. Salazar, and B. Schenke, *Nuclear geometry at high energy from exclusive vector meson production*, *Phys. Rev. D* **D106** (2022) 074019, [arXiv:2207.03712](#).
- [49] C. A. Flett *et al.*, *Exclusive J/ψ and Υ production in high energy pp and pPb collisions*, *Phys. Rev. D* **D106** (2022) 074021, [arXiv:2206.10161](#).
- [50] V. Guzey, E. Kryshen, M. Strikman, and M. Zhalov, *Nuclear suppression from coherent J/ψ photoproduction at the Large Hadron Collider*, *Phys. Lett. B* **B816** (2021) 136202, [arXiv:2008.10891](#).
- [51] C. Henkels, E. G. de Oliveira, R. Pasechnik, and H. Trebien, *Exclusive photoproduction of excited quarkonia in ultraperipheral collisions*, *Phys. Rev. D* **D102** (2020) 014024, [arXiv:2004.00607](#).
- [52] Z. Cao *et al.*, *Photoproduction of J/ψ in non-single-diffractive p+p collisions*, *Chin. Phys. C* **C43** (2019) 064103, [arXiv:1810.10685](#).
- [53] STAR collaboration, *Observation of strong nuclear suppression in exclusive J/ψ photoproduction in Au+Au ultra-peripheral collisions at RHIC*, [arXiv:2311.13637](#).
- [54] STAR collaboration, *Exclusive J/ψ , $\psi(2S)$, and e^+e^- pair production in Au+Au ultra-peripheral collisions at RHIC*, [arXiv:2311.13632](#).
- [55] ALICE collaboration, S. Acharya *et al.*, *Coherent J/ψ and ψ' photoproduction at midrapidity in ultra-peripheral Pb-Pb collisions at $\sqrt{s_{NN}} = 5.02$ TeV*, *Eur. Phys. J. C* **C81** (2021) 712, [arXiv:2101.04577](#).
- [56] ALICE collaboration, S. Acharya *et al.*, *Energy dependence of coherent photonuclear production of J/ψ mesons in ultra-peripheral Pb-Pb collisions at $\sqrt{s_{NN}} = 5.02$ TeV*, *JHEP* **10** (2023) 119, [arXiv:2305.19060](#).
- [57] X.-Y. Wang, F. Zeng, and I. I. Strakovsky, *$\psi^{(*)}p$ scattering length based on near-threshold charmonium photoproduction*, *Phys. Rev. C* **C106** (2022) 015202, [arXiv:2205.07661](#).
- [58] X.-Y. Wang, F. Zeng, and Q. Wang, *Systematic analysis of the proton mass radius based on photoproduction of vector charmoniums*, *Phys. Rev. D* **D105** (2022) 096033, [arXiv:2204.07294](#).
- [59] A. Arroyo Garcia, M. Hentschinski, and K. Kutak, *QCD evolution based evidence for the onset of gluon saturation in exclusive photo-production of vector mesons*, *Phys. Lett. B* **B795** (2019) 569, [arXiv:1904.04394](#).

- [60] LHCb collaboration, A. A. Alves Jr. *et al.*, *The LHCb detector at the LHC*, [JINST **3** \(2008\) S08005](#).
- [61] LHCb collaboration, R. Aaij *et al.*, *LHCb detector performance*, [Int. J. Mod. Phys. **A30** \(2015\) 1530022](#), [arXiv:1412.6352](#).
- [62] R. Aaij *et al.*, *Performance of the LHCb Vertex Locator*, [JINST **9** \(2014\) P09007](#), [arXiv:1405.7808](#).
- [63] P. d'Argent *et al.*, *Improved performance of the LHCb Outer Tracker in LHC Run 2*, [JINST **12** \(2017\) P11016](#), [arXiv:1708.00819](#).
- [64] A. A. Alves Jr. *et al.*, *Performance of the LHCb muon system*, [JINST **8** \(2013\) P02022](#), [arXiv:1211.1346](#).
- [65] K. Carvalho Akiba *et al.*, *The HeRSChel detector: high-rapidity shower counters for LHCb*, [JINST **13** \(2018\) P04017](#), [arXiv:1801.04281](#).
- [66] C. Sánchez Gras, *Exceptionally empty charm — Central exclusive production of charmonia at LHCb*, PhD thesis, 2022, [CERN-THESIS-2022-235](#).
- [67] R. Aaij *et al.*, *The LHCb trigger and its performance in 2011*, [JINST **8** \(2013\) P04022](#), [arXiv:1211.3055](#).
- [68] L. A. Harland-Lang, V. A. Khoze, and M. G. Ryskin, *Exclusive physics at the LHC with SuperChic 2*, [Eur. Phys. J. **C76** \(2016\) 9](#), [arXiv:1508.02718](#).
- [69] D. J. Lange, *The EvtGen particle decay simulation package*, [Nucl. Instrum. Meth. **A462** \(2001\) 152](#).
- [70] N. Davidson, T. Przedzinski, and Z. Was, *PHOTOS interface in C++: Technical and physics documentation*, [Comp. Phys. Comm. **199** \(2016\) 86](#), [arXiv:1011.0937](#).
- [71] Geant4 collaboration, J. Allison *et al.*, *Geant4 developments and applications*, [IEEE Trans. Nucl. Sci. **53** \(2006\) 270](#); Geant4 collaboration, S. Agostinelli *et al.*, *Geant4: A simulation toolkit*, [Nucl. Instrum. Meth. **A506** \(2003\) 250](#).
- [72] M. Clemencic *et al.*, *The LHCb simulation application, Gauss: Design, evolution and experience*, [J. Phys. Conf. Ser. **331** \(2011\) 032023](#).
- [73] R. Brun and F. Rademakers, *ROOT: An object oriented data analysis framework*, [Nucl. Instrum. Meth. A **389** \(1997\) 81](#).
- [74] G. Corti *et al.*, *Software for the LHCb experiment*, [IEEE Trans. Nucl. Sci. **53** \(2006\) 1323](#).
- [75] LHCb collaboration, P. Koppenburg, *Reconstruction and analysis software environment of LHCb*, [Nucl. Phys. B Proc. Suppl. **156** \(2006\) 213](#).
- [76] A. Tsaregorodtsev *et al.*, *DIRAC3: The new generation of the LHCb grid software*, [J. Phys. Conf. Ser. **219** \(2010\) 062029](#).

- [77] C. R. Harris *et al.*, *Array programming with NumPy*, *Nature* **585** (2020) 357, [arXiv:2006.10256](#).
- [78] B. Gough, *GNU scientific library reference manual*, Network Theory Ltd., 2009.
- [79] W. Verkerke and D. P. Kirkby, *The RooFit toolkit for data modeling*, eConf **C0303241** (2003) MOLT007, [arXiv:physics/0306116](#).
- [80] F. James and M. Roos, *Minuit: A system for function minimization and analysis of the parameter errors and correlations*, *Comput. Phys. Commun.* **10** (1975) 343.
- [81] J. D. Hunter, *Matplotlib: A 2D Graphics Environment*, *Comput. Sci. Eng.* **9** (2007) 90.
- [82] F. Mölder, K. P. Jablonski, B. Letcher *et al.*, *Sustainable data analysis with snake-make*, *F1000Research* (2021) 10:33.
- [83] LHCb collaboration, R. Aaij *et al.*, *Precision luminosity measurements at LHCb*, *JINST* **9** (2014) P12005, [arXiv:1410.0149](#).
- [84] T. Skwarnicki, *A study of the radiative cascade transitions between the Upsilon-prime and Upsilon resonances*, PhD thesis, Institute of Nuclear Physics, Krakow, 1986, [DESY-F31-86-02](#).
- [85] Particle Data Group, N. S. *et al.*, *Review of particle physics*, to be published in *Phys. Rev* **D110** (2024) 030001.
- [86] LHCb collaboration, R. Aaij *et al.*, *Measurement of the $B_s^0 \rightarrow \mu^+ \mu^-$ decay properties and search for the $B^0 \rightarrow \mu^+ \mu^-$ and $B_s^0 \rightarrow \mu^+ \mu^- \gamma$ decays*, *Phys. Rev.* **D105** (2022) 012010, [arXiv:2108.09283](#).
- [87] P. D. B. Collins, *An introduction to Regge theory and high-energy physics*, *Cambridge Monographs on Mathematical Physics*, Cambridge Univ. Press, Cambridge, UK, 2009.
- [88] H1 collaboration, V. Andreev *et al.*, *Determination of electroweak parameters in polarised deep-inelastic scattering at HERA*, [arXiv:1806.01176](#).
- [89] H1 collaboration, C. Alexa *et al.*, *Elastic and proton-dissociative photoproduction of J/ψ mesons at HERA*, *Eur. Phys. J.* **C73** (2013) 2466, [arXiv:1304.5162](#).
- [90] LHCb collaboration, R. Aaij *et al.*, *Fraction of χ_c decays in prompt J/ψ production measured in pPb collisions at $\sqrt{s_{NN}} = 8.16$ TeV*, *Phys. Rev. Lett.* **132** (2024) 102302, [arXiv:2311.01562](#).
- [91] S. P. Jones, A. D. Martin, M. G. Ryskin, and T. Teubner, *Probes of the small x gluon via exclusive J/ψ and Y production at HERA and the LHC*, *JHEP* **11** (2013) 085, [arXiv:1307.7099](#).
- [92] S. P. Jones, A. D. Martin, M. G. Ryskin, and T. Teubner, *Predictions of exclusive $\psi(2S)$ production at the LHC*, *J. Phys.* **G41** (2014) 055009, [arXiv:1312.6795](#).

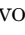




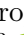
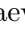

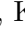

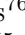

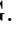
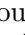
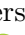
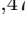

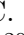
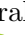
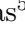







- [93] H1 collaboration, C. Adloff *et al.*, *Diffraction photoproduction of $\psi(2S)$ mesons at HERA*, *Phys. Lett.* **B541** (2002) 251, [arXiv:hep-ex/0205107](#).
- [94] ZEUS collaboration, H. Abramowicz *et al.*, *Measurement of the cross-section ratio $\sigma_{\psi(2S)}/\sigma_{J/\psi}$ in deep inelastic exclusive ep scattering at HERA*, *Nucl. Phys.* **B909** (2016) 934, [arXiv:1606.08652](#).
- [95] H1 collaboration, A. Aktas *et al.*, *Elastic J/ψ production at HERA*, *Eur. Phys. J.* **C46** (2006) 585, [arXiv:hep-ex/0510016](#).
- [96] ZEUS collaboration, S. Chekanov *et al.*, *Exclusive photoproduction of J/ψ mesons at HERA*, *Eur. Phys. J.* **C24** (2002) 345, [arXiv:hep-ex/0201043](#).
- [97] H1 collaboration, V. Andreev *et al.*, *Measurement of exclusive $\pi^+\pi^-$ and ρ meson photoproduction at HERA*, *Eur. Phys. J.* **C80** (2020) 1189, [arXiv:2005.14471](#).
- [98] A. Donnachie and P. V. Landshoff, *Charm production at HERA*, *Phys. Lett.* **B470** (1999) 243, [arXiv:hep-ph/9910262](#).
- [99] S. P. Jones, A. D. Martin, M. G. Ryskin, and T. Teubner, *Exclusive J/ψ production at the LHC in the k_T factorization approach*, *J. Phys.* **G44** (2017) 03LT01, [arXiv:1611.03711](#).
- [100] V. M. Budnev, I. F. Ginzburg, G. V. Meledin, and V. G. Serbo, *The two photon particle production mechanism. Physical problems. Applications. Equivalent photon approximation*, *Phys. Rept.* **15** (1975) 181.
- [101] O. Kepka, *QCD and Diffraction in the ATLAS Experiment at the LHC*, PhD thesis, Prague, Inst. Phys. & Orsay, 2009, Presented on 06 Nov 2009.
- [102] ALICE collaboration, B. B. Abelev *et al.*, *Exclusive J/ψ photoproduction off protons in ultra-peripheral p-Pb collisions at $\sqrt{s_{NN}} = 5.02$ TeV*, *Phys. Rev. Lett.* **113** (2014) 232504, [arXiv:1406.7819](#).
- [103] ALICE collaboration, S. Acharya *et al.*, *Energy dependence of exclusive J/ψ photoproduction off protons in ultra-peripheral p-Pb collisions at $\sqrt{s_{NN}} = 5.02$ TeV*, *Eur. Phys. J.* **C79** (2019) 402, [arXiv:1809.03235](#).
- [104] B. Knapp *et al.*, *Photoproduction of narrow resonances*, *Phys. Rev. Lett.* **34** (1975) 1040.
- [105] M. E. Binkley *et al.*, *J/ψ photoproduction from 60 GeV/c to 300 GeV/c*, *Phys. Rev. Lett.* **48** (1982) 73.
- [106] B. H. Denby *et al.*, *Inelastic and elastic photoproduction of $J/\psi(3097)$* , *Phys. Rev. Lett.* **52** (1984) 795.

LHCb collaboration

R. Aaij³⁶ , A.S.W. Abdelmotteleb⁵⁵ , C. Abellan Beteta⁴⁹ , F. Abudinén⁵⁵ ,
T. Ackernley⁵⁹ , A. A. Adefisoye⁶⁷ , B. Adeva⁴⁵ , M. Adinolfi⁵³ , P. Adlarson⁷⁹ ,
C. Agapopoulou¹³ , C.A. Aidala⁸⁰ , Z. Ajaltouni¹¹ , S. Akar⁶⁴ , K. Akiba³⁶ ,
P. Albicocco²⁶ , J. Albrecht¹⁸ , F. Alessio⁴⁷ , M. Alexander⁵⁸ , Z. Aliouche⁶¹ ,
P. Alvarez Cartelle⁵⁴ , R. Amalric¹⁵ , S. Amato³ , J.L. Amey⁵³ , Y. Amhis^{13,47} ,
L. An⁶ , L. Anderlini²⁵ , M. Andersson⁴⁹ , A. Andreianov⁴² , P. Andreola⁴⁹ ,
M. Andreotti²⁴ , D. Andreou⁶⁷ , A. Anelli^{29,p} , D. Ao⁷ , F. Archilli^{35,v} ,
M. Argenton²⁴ , S. Arguedas Cuendis⁹ , A. Artamonov⁴² , M. Artuso⁶⁷ ,
E. Aslanides¹² , R. Ataíde Da Silva⁴⁸ , M. Atzeni⁶³ , B. Audurier¹⁴ , D. Bacher⁶² ,
I. Bachiller Perea¹⁰ , S. Bachmann²⁰ , M. Bachmayer⁴⁸ , J.J. Back⁵⁵ ,
P. Baladron Rodriguez⁴⁵ , V. Balagura¹⁴ , W. Baldini²⁴ , H. Bao⁷ ,
J. Baptista de Souza Leite⁵⁹ , M. Barbetti^{25,m} , I. R. Barbosa⁶⁸ , R.J. Barlow⁶¹ ,
M. Barnyakov²³ , S. Barsuk¹³ , W. Barter⁵⁷ , M. Bartolini⁵⁴ , J. Bartz⁶⁷ ,
J.M. Basels¹⁶ , G. Bassi^{33,s} , B. Batsukh⁵ , A. Bay⁴⁸ , A. Beck⁵⁵ , M. Becker¹⁸ ,
F. Bedeschi³³ , I.B. Bediaga² , S. Belin⁴⁵ , V. Bellee⁴⁹ , K. Belous⁴² , I. Belov²⁷ ,
I. Belyaev³⁴ , G. Benane¹² , G. Bencivenni²⁶ , E. Ben-Haim¹⁵ , A. Berezhnuy⁴² ,
R. Bernet⁴⁹ , S. Bernet Andres⁴³ , A. Bertolin³¹ , C. Betancourt⁴⁹ , F. Betti⁵⁷ , J.
Bex⁵⁴ , I.a. Bezshyiko⁴⁹ , J. Bhom³⁹ , M.S. Bieker¹⁸ , N.V. Biesuz²⁴ , P. Billoir¹⁵ ,
A. Biolchini³⁶ , M. Birch⁶⁰ , F.C.R. Bishop¹⁰ , A. Bitadze⁶¹ , A. Bizzeti , T. Blake⁵⁵ ,
F. Blanc⁴⁸ , J.E. Blank¹⁸ , S. Blusk⁶⁷ , V. Bocharnikov⁴² , J.A. Boelhave¹⁸ ,
O. Boente Garcia¹⁴ , T. Boettcher⁶⁴ , A. Bohare⁵⁷ , A. Boldyrev⁴² , C.S. Bolognani⁷⁶ ,
R. Bolzonella^{24,l} , N. Bondar⁴² , F. Borgato^{31,q} , S. Borghi⁶¹ , M. Borsato^{29,p} ,
J.T. Borsuk³⁹ , S.A. Bouchiba⁴⁸ , T.J.V. Bowcock⁵⁹ , A. Boyer⁴⁷ , C. Bozzi²⁴ , P.
Braat³⁶ , A. Brea Rodriguez⁴⁸ , N. Breer¹⁸ , J. Brodzicka³⁹ ,
A. Brossa Gonzalo^{45,55,44,†} , J. Brown⁵⁹ , D. Brundu³⁰ , E. Buchanan⁵⁷ , A. Buonauro⁴⁹ ,
L. Buonincontri^{31,q} , A.T. Burke⁶¹ , C. Burr⁴⁷ , A. Butkevich⁴² , J.S. Butter⁵⁴ ,
J. Buytaert⁴⁷ , W. Byczynski⁴⁷ , S. Cadeddu³⁰ , H. Cai⁷² , R. Calabrese^{24,l} ,
S. Calderon Ramirez⁹ , L. Calefice⁴⁴ , S. Cali²⁶ , M. Calvi^{29,p} , M. Calvo Gomez⁴³ ,
P. Camargo Magalhaes^{2,z} , J. I. Cambon Bouzas⁴⁵ , P. Campana²⁶ ,
D.H. Campora Perez⁷⁶ , A.F. Campoverde Quezada⁷ , S. Capelli²⁹ , L. Capriotti²⁴ ,
R. Caravaca-Mora⁹ , A. Carbone^{23,j} , L. Carcedo Salgado⁴⁵ , R. Cardinale^{27,n} ,
A. Cardini³⁰ , P. Carniti^{29,p} , L. Carus²⁰ , A. Casais Vidal⁶³ , R. Caspary²⁰ ,
G. Casse⁵⁹ , J. Castro Godinez⁹ , M. Cattaneo⁴⁷ , G. Cavallero^{24,47} , V. Cavallini^{24,l} ,
S. Celani²⁰ , D. Cervenkov⁶² , S. Cesare^{28,o} , A.J. Chadwick⁵⁹ , I. Chahrour⁸⁰ ,
M. Charles¹⁵ , Ph. Charpentier⁴⁷ , E. Chatzianagnostou³⁶ , C.A. Chavez Barajas⁵⁹ ,
M. Chefdeville¹⁰ , C. Chen¹² , S. Chen⁵ , Z. Chen⁷ , A. Chernov³⁹ ,
S. Chernyshenko⁵¹ , V. Chobanova⁷⁸ , S. Cholak⁴⁸ , M. Chrzaszcz³⁹ , A. Chubykin⁴² ,
V. Chulikov⁴² , P. Ciambriano²⁶ , X. Cid Vidal⁴⁵ , G. Ciezarek⁴⁷ , P. Cifra⁴⁷ ,
P.E.L. Clarke⁵⁷ , M. Clemencic⁴⁷ , H.V. Cliff⁵⁴ , J. Closier⁴⁷ , C. Cocha Toapaxi²⁰ ,
V. Coco⁴⁷ , J. Cogan¹² , E. Cogneras¹¹ , L. Cojocariu⁴¹ , P. Collins⁴⁷ ,
T. Colombo⁴⁷ , A. Comerma-Montells⁴⁴ , L. Congedo²² , A. Contu³⁰ , N. Cooke⁵⁸ ,
I. Corredoira⁴⁵ , A. Correia¹⁵ , G. Corti⁴⁷ , J.J. Cottee Meldrum⁵³ , B. Couturier⁴⁷ ,
D.C. Craik⁴⁹ , M. Cruz Torres^{2,g} , E. Curras Rivera⁴⁸ , R. Currie⁵⁷ , C.L. Da Silva⁶⁶ ,
S. Dadabaev⁴² , L. Dai⁶⁹ , X. Dai⁶ , E. Dall’Occo¹⁸ , J. Dalseno⁴⁵ ,
C. D’Ambrosio⁴⁷ , J. Daniel¹¹ , A. Danilina⁴² , P. d’Argent²² , A. Davidson⁵⁵ ,
J.E. Davies⁶¹ , A. Davis⁶¹ , O. De Aguiar Francisco⁶¹ , C. De Angelis^{30,k} ,
F. De Benedetti⁴⁷ , J. de Boer³⁶ , K. De Bruyn⁷⁵ , S. De Capua⁶¹ , M. De Cian^{20,47} ,
U. De Freitas Carneiro Da Graca^{2,b} , E. De Lucia²⁶ , J.M. De Miranda² , L. De Paula³

M. De Serio^{22,h} , P. De Simone²⁶ , F. De Vellis¹⁸ , J.A. de Vries⁷⁶ , F. Debernardis²² ,
 D. Decamp¹⁰ , V. Dedu¹² , L. Del Buono¹⁵ , B. Delaney⁶³ , H.-P. Dembinski¹⁸ ,
 J. Deng⁸ , V. Denysenko⁴⁹ , O. Deschamps¹¹ , F. Dettori^{30,k} , B. Dey⁷⁴ ,
 P. Di Nezza²⁶ , I. Diachkov⁴² , S. Didenko⁴² , S. Ding⁶⁷ , L. Dittmann²⁰ ,
 V. Dobishuk⁵¹ , A. D. Docheva⁵⁸ , C. Dong⁴ , A.M. Donohoe²¹ , F. Dordei³⁰ ,
 A.C. dos Reis² , A. D. Dowling⁶⁷ , W. Duan⁷⁰ , P. Duda⁷⁷ , M.W. Dudek³⁹ ,
 L. Dufour⁴⁷ , V. Duk³² , P. Durante⁴⁷ , M. M. Duras⁷⁷ , J.M. Durham⁶⁶ , O. D.
 Durmus⁷⁴ , A. Dziurda³⁹ , A. Dzyuba⁴² , S. Easo⁵⁶ , E. Eckstein¹⁷ , U. Egede¹ ,
 A. Egorychev⁴² , V. Egorychev⁴² , S. Eisenhardt⁵⁷ , E. Ejopu⁶¹ , L. Eklund⁷⁹ ,
 M. Elashri⁶⁴ , J. Ellbracht¹⁸ , S. Ely⁶⁰ , A. Ene⁴¹ , E. Epple⁶⁴ , J. Eschle⁶⁷ ,
 S. Esen²⁰ , T. Evans⁶¹ , F. Fabiano^{30,k} , L.N. Falcao² , Y. Fan⁷ , B. Fang⁷² ,
 L. Fantini^{32,r,47} , M. Faria⁴⁸ , K. Farmer⁵⁷ , D. Fazzini^{29,p} , L. Felkowski⁷⁷ ,
 M. Feng^{5,7} , M. Feo^{18,47} , M. Fernandez Gomez⁴⁵ , A.D. Fernez⁶⁵ , F. Ferrari²³ ,
 F. Ferreira Rodrigues³ , M. Ferrillo⁴⁹ , M. Ferro-Luzzi⁴⁷ , S. Filippov⁴² , R.A. Fini²² ,
 M. Fiorini^{24,l} , K.L. Fischer⁶² , D.S. Fitzgerald⁸⁰ , C. Fitzpatrick⁶¹ , F. Fleuret¹⁴ ,
 M. Fontana²³ , L. F. Foreman⁶¹ , R. Forty⁴⁷ , D. Foulds-Holt⁵⁴ , M. Franco Sevilla⁶⁵ ,
 M. Frank⁴⁷ , E. Franzoso^{24,l} , G. Frau⁶¹ , C. Frei⁴⁷ , D.A. Friday⁶¹ , J. Fu⁷ ,
 Q. Fuehring¹⁸ , Y. Fujii¹ , T. Fulghesu¹⁵ , E. Gabriel³⁶ , G. Galati²² , M.D. Galati³⁶ ,
 A. Gallas Torreira⁴⁵ , D. Galli^{23,j} , S. Gambetta⁵⁷ , M. Gandelman³ , P. Gandini²⁸ , B.
 Ganie⁶¹ , H. Gao⁷ , R. Gao⁶² , Y. Gao⁸ , Y. Gao⁶ , Y. Gao⁸ , M. Garau^{30,k} ,
 L.M. Garcia Martin⁴⁸ , P. Garcia Moreno⁴⁴ , J. García Pardiñas⁴⁷ , K. G. Garg⁸ ,
 L. Garrido⁴⁴ , C. Gaspar⁴⁷ , R.E. Geertsema³⁶ , L.L. Gerken¹⁸ , E. Gersabeck⁶¹ ,
 M. Gersabeck⁶¹ , T. Gershon⁵⁵ , Z. Ghorbanimoghaddam⁵³ , L. Giambastiani^{31,q} , F.
 I. Giasemis^{15,e} , V. Gibson⁵⁴ , H.K. Giemza⁴⁰ , A.L. Gilman⁶² , M. Giovannetti²⁶ ,
 A. Gioventù⁴⁴ , P. Gironella Gironell⁴⁴ , C. Giugliano^{24,l} , M.A. Giza³⁹ ,
 E.L. Gkoukousis⁶⁰ , F.C. Glaser^{13,20} , V.V. Gligorov^{15,47} , C. Göbel⁶⁸ ,
 E. Golobardes⁴³ , D. Golubkov⁴² , A. Golutvin^{60,42,47} , A. Gomes^{2,a,†} ,
 S. Gomez Fernandez⁴⁴ , F. Goncalves Abrantes⁶² , M. Goncerz³⁹ , G. Gong⁴ , J.
 A. Gooding¹⁸ , I.V. Gorelov⁴² , C. Gotti²⁹ , J.P. Grabowski¹⁷ ,
 L.A. Granado Cardoso⁴⁷ , E. Graugés⁴⁴ , E. Graverini^{48,t} , L. Grazette⁵⁵ ,
 G. Graziani , A. T. Grecu⁴¹ , L.M. Greeven³⁶ , N.A. Grieser⁶⁴ , L. Grillo⁵⁸ ,
 S. Gromov⁴² , C. Gu¹⁴ , M. Guarise²⁴ , M. Guittiere¹³ , V. Guliaeva⁴² , P.
 A. Günther²⁰ , A.-K. Guseinov⁴⁸ , E. Gushchin⁴² , Y. Guz^{6,42,47} , T. Gys⁴⁷ ,
 K. Habermann¹⁷ , T. Hadavizadeh¹ , C. Hadjivasiliou⁶⁵ , G. Haefeli⁴⁸ , C. Haen⁴⁷ ,
 J. Haimberger⁴⁷ , M. Hajheidari⁴⁷ , M.M. Halvorsen⁴⁷ , P.M. Hamilton⁶⁵ ,
 J. Hammerich⁵⁹ , Q. Han⁸ , X. Han²⁰ , S. Hansmann-Menzemer²⁰ , L. Hao⁷ ,
 N. Harnew⁶² , M. Hartmann¹³ , J. He^{7,c} , F. Hemmer⁴⁷ , C. Henderson⁶⁴ ,
 R.D.L. Henderson^{1,55} , A.M. Hennequin⁴⁷ , K. Hennessy⁵⁹ , L. Henry⁴⁸ , J. Herd⁶⁰ ,
 P. Herrero Gascon²⁰ , J. Heuel¹⁶ , A. Hicheur³ , G. Hijano Mendizabal⁴⁹ , D. Hill⁴⁸ ,
 S.E. Hollitt¹⁸ , J. Horswill⁶¹ , R. Hou⁸ , Y. Hou¹¹ , N. Howarth⁵⁹ , J. Hu²⁰ , J. Hu⁷⁰ ,
 W. Hu⁶ , X. Hu⁴ , W. Huang⁷ , W. Hulsbergen³⁶ , R.J. Hunter⁵⁵ , M. Hushchyn⁴² ,
 D. Hutchcroft⁵⁹ , D. Ilin⁴² , P. Ilten⁶⁴ , A. Inglessi⁴² , A. Iniukhin⁴² , A. Ishteev⁴² ,
 K. Ivshin⁴² , R. Jacobsson⁴⁷ , H. Jage¹⁶ , S.J. Jaimes Elles^{46,73} , S. Jakobsen⁴⁷ ,
 E. Jans³⁶ , B.K. Jashal⁴⁶ , A. Jawahery^{65,47} , V. Jevtic¹⁸ , E. Jiang⁶⁵ , X. Jiang^{5,7} ,
 Y. Jiang⁷ , Y. J. Jiang⁶ , M. John⁶² , D. Johnson⁵² , C.R. Jones⁵⁴ , T.P. Jones⁵⁵ ,
 S. Joshi⁴⁰ , B. Jost⁴⁷ , N. Jurik⁴⁷ , I. Juszczak³⁹ , D. Kaminaris⁴⁸ , S. Kandybei⁵⁰ ,
 M. Kane⁵⁷ , Y. Kang⁴ , C. Kar¹¹ , M. Karacson⁴⁷ , D. Karpenkov⁴² ,
 A. Kauniskangas⁴⁸ , J.W. Kautz⁶⁴ , F. Keizer⁴⁷ , M. Kenzie⁵⁴ , T. Ketel³⁶ ,
 B. Khanji⁶⁷ , A. Kharisova⁴² , S. Kholodenko^{33,47} , G. Khreich¹³ , T. Kirn¹⁶ ,
 V.S. Kirsebom^{29,p} , O. Kitouni⁶³ , S. Klaver³⁷ , N. Kleijne^{33,s} , K. Klimaszewski⁴⁰ ,

M.R. Kmiec⁴⁰ , S. Koliiev⁵¹ , L. Kolk¹⁸ , A. Konoplyannikov⁴² , P. Kopciwicz^{38,47} ,
P. Koppenburg³⁶ , M. Korolev⁴² , I. Kostiuk³⁶ , O. Kot⁵¹ , S. Kotriakhova ,
A. Kozachuk⁴² , P. Kravchenko⁴² , L. Kravchuk⁴² , M. Kreps⁵⁵ , P. Krokovny⁴² ,
W. Krupa⁶⁷ , W. Krzemien⁴⁰ , O.K. Kshyvanskiy⁵¹ , J. Kubat²⁰ , S. Kubis⁷⁷ ,
M. Kucharczyk³⁹ , V. Kudryavtsev⁴² , E. Kulikova⁴² , A. Kupsc⁷⁹ , B. K. Kutsenko¹² ,
D. Lacarrere⁴⁷ , A. Lai³⁰ , A. Lampis³⁰ , D. Lancierini⁵⁴ , C. Landesa Gomez⁴⁵ ,
J.J. Lane¹ , R. Lane⁵³ , C. Langenbruch²⁰ , J. Langer¹⁸ , O. Lantwin⁴² ,
T. Latham⁵⁵ , F. Lazzari^{33,t} , C. Lazzaroni⁵² , R. Le Gac¹² , R. Lefèvre¹¹ ,
A. Leflat⁴² , S. Legotin⁴² , M. Lehuraux⁵⁵ , E. Lemos Cid⁴⁷ , O. Leroy¹² ,
T. Lesiak³⁹ , B. Leverington²⁰ , A. Li⁴ , H. Li⁷⁰ , K. Li⁸ , L. Li⁶¹ , P. Li⁴⁷ ,
P.-R. Li⁷¹ , Q. Li^{5,7} , S. Li⁸ , T. Li^{5,d} , T. Li⁷⁰ , Y. Li⁸ , Y. Li⁵ , Z. Lian⁴ ,
X. Liang⁶⁷ , S. Libralon⁴⁶ , C. Lin⁷ , T. Lin⁵⁶ , R. Lindner⁴⁷ , V. Lisovskyi⁴⁸ ,
R. Litvinov^{30,47} , F. L. Liu¹ , G. Liu⁷⁰ , K. Liu⁷¹ , S. Liu^{5,7} , Y. Liu⁵⁷ , Y. Liu⁷¹ ,
L. Liu⁶⁰ , A. Lobo Salvia⁴⁴ , A. Loi³⁰ , J. Lomba Castro⁴⁵ , T. Long⁵⁴ ,
J.H. Lopes³ , A. Lopez Huertas⁴⁴ , S. López Soliño⁴⁵ , A. Loya Villalpando³⁶ ,
C. Lucarelli^{25,m} , D. Lucchesi^{31,q} , M. Lucio Martinez⁷⁶ , V. Lukashenko^{36,51} ,
Y. Luo⁶ , A. Lupato³¹ , E. Luppi^{24,l} , K. Lynch²¹ , X.-R. Lyu⁷ , G. M. Ma⁴ ,
R. Ma⁷ , S. Maccolini¹⁸ , F. Machefert¹³ , F. Maciuc⁴¹ , B. Mack⁶⁷ , I. Mackay⁶² , L.
M. Mackey⁶⁷ , L.R. Madhan Mohan⁵⁴ , M. J. Madurai⁵² , A. Maevskiy⁴² ,
D. Magdalinski³⁶ , D. Maisuzenko⁴² , M.W. Majewski³⁸ , J.J. Malczewski³⁹ , S. Malde⁶² ,
L. Malentacca⁴⁷ , A. Malinin⁴² , T. Maltsev⁴² , G. Manca^{30,k} , G. Mancinelli¹² ,
C. Mancuso^{28,13,o} , R. Manera Escalero⁴⁴ , D. Manuzzi²³ , D. Marangotto^{28,o} ,
J.F. Marchand¹⁰ , R. Marcheviski⁴⁸ , U. Marconi²³ , S. Mariani⁴⁷ , C. Marin Benito⁴⁴ ,
J. Marks²⁰ , A.M. Marshall⁵³ , G. Martelli^{32,r} , G. Martellotti³⁴ , L. Martinazzoli⁴⁷ ,
M. Martinelli^{29,p} , D. Martinez Santos⁴⁵ , F. Martinez Vidal⁴⁶ , A. Massafferri² ,
R. Matev⁴⁷ , A. Mathad⁴⁷ , V. Matiunin⁴² , C. Matteuzzi⁶⁷ , K.R. Mattioli¹⁴ ,
A. Mauri⁶⁰ , E. Maurice¹⁴ , J. Mauricio⁴⁴ , P. Mayencourt⁴⁸ , M. Mazurek⁴⁰ ,
M. McCann⁶⁰ , L. McConnell²¹ , T.H. McGrath⁶¹ , N.T. McHugh⁵⁸ , A. McNab⁶¹ ,
R. McNulty²¹ , B. Meadows⁶⁴ , G. Meier¹⁸ , D. Melnychuk⁴⁰ , F. M. Meng⁴ ,
M. Merk^{36,76} , A. Merli⁴⁸ , L. Meyer Garcia⁶⁵ , D. Miao^{5,7} , H. Miao⁷ ,
M. Mikhasenko^{17,f} , D.A. Milanese⁷³ , A. Minotti^{29,p} , E. Minucci⁶⁷ , T. Miralles¹¹ ,
B. Mitreska¹⁸ , D.S. Mittel¹⁸ , A. Modak⁵⁶ , A. Mödden¹⁸ , R.A. Mohammed⁶² ,
R.D. Moise¹⁶ , S. Mokhnenko⁴² , T. Mombächer⁴⁷ , M. Monk^{55,1} , S. Monteil¹¹ ,
A. Morcillo Gomez⁴⁵ , G. Morello²⁶ , M.J. Morello^{33,s} , M.P. Morgenthaler²⁰ ,
A.B. Morris⁴⁷ , A.G. Morris¹² , R. Mountain⁶⁷ , H. Mu⁴ , Z. M. Mu⁶ ,
E. Muhammad⁵⁵ , F. Muheim⁵⁷ , M. Mulder⁷⁵ , K. Müller⁴⁹ , F. Muñoz-Rojas⁹ ,
R. Murta⁶⁰ , P. Naik⁵⁹ , T. Nakada⁴⁸ , R. Nandakumar⁵⁶ , T. Nanut⁴⁷ , I. Nasteva³ ,
M. Needham⁵⁷ , N. Neri^{28,o} , S. Neubert¹⁷ , N. Neufeld⁴⁷ , P. Neustroev⁴² ,
J. Nicolini^{18,13} , D. Nicotra⁷⁶ , E.M. Niel⁴⁸ , N. Nikitin⁴² , P. Nogaroli³ , P. Nogga¹⁷ ,
N.S. Nolte⁶³ , C. Normand⁵³ , J. Novoa Fernandez⁴⁵ , G. Nowak⁶⁴ , C. Nunez⁸⁰ , H. N.
Nur⁵⁸ , A. Oblakowska-Mucha³⁸ , V. Obraztsov⁴² , T. Oeser¹⁶ , S. Okamura^{24,l} ,
A. Okhotnikov⁴² , O. Okhrimenko⁵¹ , R. Oldeman^{30,k} , F. Oliva⁵⁷ , M. Olocco¹⁸ ,
C.J.G. Onderwater⁷⁶ , R.H. O'Neil⁵⁷ , J.M. Otalora Goicochea³ , P. Owen⁴⁹ ,
A. Oyanguren⁴⁶ , O. Ozcelik⁵⁷ , A. Padee⁴⁰ , K.O. Padeken¹⁷ , B. Pagare⁵⁵ ,
P.R. Pais²⁰ , T. Pajero⁴⁷ , A. Palano²² , M. Palutan²⁶ , G. Panshin⁴² , L. Paolucci⁵⁵ ,
A. Papanestis⁵⁶ , M. Pappagallo^{22,h} , L.L. Pappalardo^{24,l} , C. Pappenheimer⁶⁴ ,
C. Parkes⁶¹ , B. Passalacqua²⁴ , G. Passaleva²⁵ , D. Passaro^{33,s} , A. Pastore²² ,
M. Patel⁶⁰ , J. Patoc⁶² , C. Patrignani^{23,j} , A. Paul⁶⁷ , C.J. Pawley⁷⁶ ,
A. Pellegrino³⁶ , J. Peng^{5,7} , M. Pepe Altarelli²⁶ , S. Perazzini²³ , D. Pereima⁴² , H.
Pereira Da Costa⁶⁶ , A. Pereiro Castro⁴⁵ , P. Perret¹¹ , A. Perro⁴⁷ , K. Petridis⁵³ ,

D. vom Bruch¹² , N. Voropaev⁴² , K. Vos⁷⁶ , G. Vouters^{10,47} , C. Vrahas⁵⁷ ,
J. Wagner¹⁸ , J. Walsh³³ , E.J. Walton^{1,55} , G. Wan⁶ , C. Wang²⁰ , G. Wang⁸ ,
J. Wang⁶ , J. Wang⁵ , J. Wang⁴ , J. Wang⁷² , M. Wang²⁸ , N. W. Wang⁷ ,
R. Wang⁵³ , X. Wang⁸ , X. Wang⁷⁰ , X. W. Wang⁶⁰ , Y. Wang⁶ , Z. Wang¹³ ,
Z. Wang⁴ , Z. Wang²⁸ , J.A. Ward^{55,1} , M. Waterlaet⁴⁷ , N.K. Watson⁵² ,
D. Websdale⁶⁰ , Y. Wei⁶ , J. Wendel⁷⁸ , B.D.C. Westhenry⁵³ , D.J. White⁶¹ ,
M. Whitehead⁵⁸ , E. Whiter⁵² , A.R. Wiederhold⁵⁵ , D. Wiedner¹⁸ , G. Wilkinson⁶² ,
M.K. Wilkinson⁶⁴ , M. Williams⁶³ , M.R.J. Williams⁵⁷ , R. Williams⁵⁴ ,
F.F. Wilson⁵⁶ , W. Wislicki⁴⁰ , M. Witek³⁹ , L. Witola²⁰ , C.P. Wong⁶⁶ ,
G. Wormser¹³ , S.A. Wotton⁵⁴ , H. Wu⁶⁷ , J. Wu⁸ , Y. Wu⁶ , Z. Wu⁷ ,
K. Wyllie⁴⁷ , S. Xian⁷⁰ , Z. Xiang⁵ , Y. Xie⁸ , A. Xu³³ , J. Xu⁷ , L. Xu⁴ , L. Xu⁴ ,
M. Xu⁵⁵ , Z. Xu¹¹ , Z. Xu⁷ , Z. Xu⁵ , D. Yang , K. Yang⁶⁰ , S. Yang⁷ ,
X. Yang⁶ , Y. Yang^{27,n} , Z. Yang⁶ , Z. Yang⁶⁵ , V. Yeroshenko¹³ , H. Yeung⁶¹ ,
H. Yin⁸ , C. Y. Yu⁶ , J. Yu⁶⁹ , X. Yuan⁵ , E. Zaffaroni⁴⁸ , M. Zavertyaev¹⁹ ,
M. Zdybal³⁹ , C. Zeng^{5,7} , M. Zeng⁴ , C. Zhang⁶ , D. Zhang⁸ , J. Zhang⁷ ,
L. Zhang⁴ , S. Zhang⁶⁹ , S. Zhang⁶ , Y. Zhang⁶ , Y. Z. Zhang⁴ , Y. Zhao²⁰ ,
A. Zharkova⁴² , A. Zhelezov²⁰ , S. Z. Zheng⁶ , X. Z. Zheng⁴ , Y. Zheng⁷ ,
T. Zhou⁶ , X. Zhou⁸ , Y. Zhou⁷ , V. Zhovkovska⁵⁵ , L. Z. Zhu⁷ , X. Zhu⁴ ,
X. Zhu⁸ , V. Zhukov¹⁶ , J. Zhuo⁴⁶ , Q. Zou^{5,7} , D. Zuliani^{31,q} , G. Zunica⁴⁸ .

¹*School of Physics and Astronomy, Monash University, Melbourne, Australia*

²*Centro Brasileiro de Pesquisas Físicas (CBPF), Rio de Janeiro, Brazil*

³*Universidade Federal do Rio de Janeiro (UFRJ), Rio de Janeiro, Brazil*

⁴*Center for High Energy Physics, Tsinghua University, Beijing, China*

⁵*Institute Of High Energy Physics (IHEP), Beijing, China*

⁶*School of Physics State Key Laboratory of Nuclear Physics and Technology, Peking University, Beijing, China*

⁷*University of Chinese Academy of Sciences, Beijing, China*

⁸*Institute of Particle Physics, Central China Normal University, Wuhan, Hubei, China*

⁹*Consejo Nacional de Rectores (CONARE), San Jose, Costa Rica*

¹⁰*Université Savoie Mont Blanc, CNRS, IN2P3-LAPP, Annecy, France*

¹¹*Université Clermont Auvergne, CNRS/IN2P3, LPC, Clermont-Ferrand, France*

¹²*Aix Marseille Univ, CNRS/IN2P3, CPPM, Marseille, France*

¹³*Université Paris-Saclay, CNRS/IN2P3, IJCLab, Orsay, France*

¹⁴*Laboratoire Leprince-Ringuet, CNRS/IN2P3, Ecole Polytechnique, Institut Polytechnique de Paris, Palaiseau, France*

¹⁵*LPNHE, Sorbonne Université, Paris Diderot Sorbonne Paris Cité, CNRS/IN2P3, Paris, France*

¹⁶*I. Physikalisches Institut, RWTH Aachen University, Aachen, Germany*

¹⁷*Universität Bonn - Helmholtz-Institut für Strahlen und Kernphysik, Bonn, Germany*

¹⁸*Fakultät Physik, Technische Universität Dortmund, Dortmund, Germany*

¹⁹*Max-Planck-Institut für Kernphysik (MPIK), Heidelberg, Germany*

²⁰*Physikalisches Institut, Ruprecht-Karls-Universität Heidelberg, Heidelberg, Germany*

²¹*School of Physics, University College Dublin, Dublin, Ireland*

²²*INFN Sezione di Bari, Bari, Italy*

²³*INFN Sezione di Bologna, Bologna, Italy*

²⁴*INFN Sezione di Ferrara, Ferrara, Italy*

²⁵*INFN Sezione di Firenze, Firenze, Italy*

²⁶*INFN Laboratori Nazionali di Frascati, Frascati, Italy*

²⁷*INFN Sezione di Genova, Genova, Italy*

²⁸*INFN Sezione di Milano, Milano, Italy*

²⁹*INFN Sezione di Milano-Bicocca, Milano, Italy*

³⁰*INFN Sezione di Cagliari, Monserrato, Italy*

³¹*INFN Sezione di Padova, Padova, Italy*

³²*INFN Sezione di Perugia, Perugia, Italy*

- ³³ INFN Sezione di Pisa, Pisa, Italy
- ³⁴ INFN Sezione di Roma La Sapienza, Roma, Italy
- ³⁵ INFN Sezione di Roma Tor Vergata, Roma, Italy
- ³⁶ Nikhef National Institute for Subatomic Physics, Amsterdam, Netherlands
- ³⁷ Nikhef National Institute for Subatomic Physics and VU University Amsterdam, Amsterdam, Netherlands
- ³⁸ AGH - University of Krakow, Faculty of Physics and Applied Computer Science, Kraków, Poland
- ³⁹ Henryk Niewodniczanski Institute of Nuclear Physics Polish Academy of Sciences, Kraków, Poland
- ⁴⁰ National Center for Nuclear Research (NCBJ), Warsaw, Poland
- ⁴¹ Horia Hulubei National Institute of Physics and Nuclear Engineering, Bucharest-Magurele, Romania
- ⁴² Affiliated with an institute covered by a cooperation agreement with CERN
- ⁴³ DS4DS, La Salle, Universitat Ramon Llull, Barcelona, Spain
- ⁴⁴ ICCUB, Universitat de Barcelona, Barcelona, Spain
- ⁴⁵ Instituto Galego de Física de Altas Enerxías (IGFAE), Universidade de Santiago de Compostela, Santiago de Compostela, Spain
- ⁴⁶ Instituto de Física Corpuscular, Centro Mixto Universidad de Valencia - CSIC, Valencia, Spain
- ⁴⁷ European Organization for Nuclear Research (CERN), Geneva, Switzerland
- ⁴⁸ Institute of Physics, Ecole Polytechnique Fédérale de Lausanne (EPFL), Lausanne, Switzerland
- ⁴⁹ Physik-Institut, Universität Zürich, Zürich, Switzerland
- ⁵⁰ NSC Kharkiv Institute of Physics and Technology (NSC KIPT), Kharkiv, Ukraine
- ⁵¹ Institute for Nuclear Research of the National Academy of Sciences (KINR), Kyiv, Ukraine
- ⁵² School of Physics and Astronomy, University of Birmingham, Birmingham, United Kingdom
- ⁵³ H.H. Wills Physics Laboratory, University of Bristol, Bristol, United Kingdom
- ⁵⁴ Cavendish Laboratory, University of Cambridge, Cambridge, United Kingdom
- ⁵⁵ Department of Physics, University of Warwick, Coventry, United Kingdom
- ⁵⁶ STFC Rutherford Appleton Laboratory, Didcot, United Kingdom
- ⁵⁷ School of Physics and Astronomy, University of Edinburgh, Edinburgh, United Kingdom
- ⁵⁸ School of Physics and Astronomy, University of Glasgow, Glasgow, United Kingdom
- ⁵⁹ Oliver Lodge Laboratory, University of Liverpool, Liverpool, United Kingdom
- ⁶⁰ Imperial College London, London, United Kingdom
- ⁶¹ Department of Physics and Astronomy, University of Manchester, Manchester, United Kingdom
- ⁶² Department of Physics, University of Oxford, Oxford, United Kingdom
- ⁶³ Massachusetts Institute of Technology, Cambridge, MA, United States
- ⁶⁴ University of Cincinnati, Cincinnati, OH, United States
- ⁶⁵ University of Maryland, College Park, MD, United States
- ⁶⁶ Los Alamos National Laboratory (LANL), Los Alamos, NM, United States
- ⁶⁷ Syracuse University, Syracuse, NY, United States
- ⁶⁸ Pontifícia Universidade Católica do Rio de Janeiro (PUC-Rio), Rio de Janeiro, Brazil, associated to ³
- ⁶⁹ School of Physics and Electronics, Hunan University, Changsha City, China, associated to ⁸
- ⁷⁰ Guangdong Provincial Key Laboratory of Nuclear Science, Guangdong-Hong Kong Joint Laboratory of Quantum Matter, Institute of Quantum Matter, South China Normal University, Guangzhou, China, associated to ⁴
- ⁷¹ Lanzhou University, Lanzhou, China, associated to ⁵
- ⁷² School of Physics and Technology, Wuhan University, Wuhan, China, associated to ⁴
- ⁷³ Departamento de Física, Universidad Nacional de Colombia, Bogota, Colombia, associated to ¹⁵
- ⁷⁴ Eotvos Lorand University, Budapest, Hungary, associated to ⁴⁷
- ⁷⁵ Van Swinderen Institute, University of Groningen, Groningen, Netherlands, associated to ³⁶
- ⁷⁶ Universiteit Maastricht, Maastricht, Netherlands, associated to ³⁶
- ⁷⁷ Tadeusz Kosciuszko Cracow University of Technology, Cracow, Poland, associated to ³⁹
- ⁷⁸ Universidade da Coruña, A Coruna, Spain, associated to ⁴³
- ⁷⁹ Department of Physics and Astronomy, Uppsala University, Uppsala, Sweden, associated to ⁵⁸
- ⁸⁰ University of Michigan, Ann Arbor, MI, United States, associated to ⁶⁷
- ⁸¹ Département de Physique Nucléaire (DPhN), Gif-Sur-Yvette, France

^a Universidade de Brasília, Brasília, Brazil

^b Centro Federal de Educação Tecnológica Celso Suckow da Fonseca, Rio De Janeiro, Brazil

^c Hangzhou Institute for Advanced Study, UCAS, Hangzhou, China

- ^d*School of Physics and Electronics, Henan University , Kaifeng, China*
^e*LIP6, Sorbonne Université, Paris, France*
^f*Excellence Cluster ORIGINS, Munich, Germany*
^g*Universidad Nacional Autónoma de Honduras, Tegucigalpa, Honduras*
^h*Università di Bari, Bari, Italy*
ⁱ*Università di Bergamo, Bergamo, Italy*
^j*Università di Bologna, Bologna, Italy*
^k*Università di Cagliari, Cagliari, Italy*
^l*Università di Ferrara, Ferrara, Italy*
^m*Università di Firenze, Firenze, Italy*
ⁿ*Università di Genova, Genova, Italy*
^o*Università degli Studi di Milano, Milano, Italy*
^p*Università degli Studi di Milano-Bicocca, Milano, Italy*
^q*Università di Padova, Padova, Italy*
^r*Università di Perugia, Perugia, Italy*
^s*Scuola Normale Superiore, Pisa, Italy*
^t*Università di Pisa, Pisa, Italy*
^u*Università della Basilicata, Potenza, Italy*
^v*Università di Roma Tor Vergata, Roma, Italy*
^w*Università di Siena, Siena, Italy*
^x*Università di Urbino, Urbino, Italy*
^y*Universidad de Alcalá, Alcalá de Henares , Spain*
^z*Facultad de Ciencias Físicas, Madrid, Spain*
^{aa}*Department of Physics/Division of Particle Physics, Lund, Sweden*
[†]*Deceased*